CHAPTER - 4

Conformations and investigation of intermolecular S-centered H-bonding in dimers and trimers clusters of thioglycolic acid (TGA)

4.1 Introduction

Mercaptoacetic acid, commonly known as thioglycolic acid (TGA), has garnered significant applications across various industries. It plays a vital role in the leather industry, where it is employed for depilation, fabric dyeing, and cosmetics, specifically in hair perming procedures.[1–4] Nonetheless, despite its extensive use in industrial settings, prolonged or acute exposure to TGA can lead to adverse health consequences.[5,6] Furthermore, thioglycolic acid (TGA) demonstrates remarkable versatility in the realm of materials science. It serves as a fundamental building block for polymer synthesis and finds wide-ranging utility in the detection of heavy metals and surface modification processes.[7–16]

In 1995, Yamaguchi et al. measured the microwave spectra of TGA and concluded therefrom that the mercapto-H group is involved in weak intramolecular hydrogen bonding, potentially allowing peripheral atoms to tunnel through low potential barriers associated with the twisting of C-S and C-C bonds.[17] Subsequently, Caminati et al.[18] employed the free jet expansion technique to reassign the rotational spectrum of TGA after observing significant variations in the spectroscopic parameters between the two states of TGA previously reported by Yamaguchi et al. In 2002, Fantoni et al. conducted computational investigations utilizing various ab initio methods[19] to analyze the conformation and S-H inversion barrier of TGA. Their findings indicated a low energy barrier for TGA, aligning with the experimental observations made by Caminati et al. Additionally, Fantoni et al. identified a second conformer of TGA at B3LYP/6-31G** and MP2/6-31G** levels, which exhibited a slightly higher energy of 0.4 kcal/mol. Since then, no further experimental or computational studies have explored the conformational space of TGA.

In this study, the conformational space of TGA was reexamined using a higher level of theory, namely the CCSD method with the cc-pVTZ basis set. The investigation revealed a consistent low energy barrier similar to previous findings. Notably, the energy difference between the second conformer of TGA was determined to be only 0.16

kcal/mol at the CCSD/cc-pVDZ level of theory. Additionally, the calculated rotational constants at this particular level closely aligned with earlier reported experimental results, suggesting the increased accuracy of the CCSD method for conformational analysis. Moreover, hydrogen bonds are widely recognized for their crucial role in various physical, chemical, and biological phenomena.[20–23] While oxygen is commonly associated with hydrogen bonding, other atoms such as carbon, nitrogen, sulfur, and selenium can also participate in weak hydrogen bond formations.[24–26] Though there has been limited research conducted on sulfur-centered hydrogen bonding[27–31] in comparison to conventional H-bonding.

Thus, due to the presence of both -SH and -OH groups in TGA, it becomes intriguing to investigate the donor and acceptor capabilities of sulfur and oxygen atoms in the formation of sulfur-centered intramolecular/intermolecular hydrogen bonds within TGA and its clusters. Analyzing such interactions is crucial for predicting the stability of TGA clusters and understanding the role played by non-covalent interactions. Therefore, some calculations were performed to investigate the properties of weak hydrogen bonds in more detail. The AIM (Atoms in Molecule) analysis was conducted to evaluate the binding energy of these bonds. Furthermore, the Non-Covalent Interaction (NCI) method was employed to visualize the weak non-covalent bonds present. Natural Bond Orbital (NBO) calculations provided valuable information regarding the role of both oxygen and sulfur atoms as donor atoms in the formation of these weak hydrogen bonds. Moreover, Frontier Molecular Orbital (FMO) calculations and charge calculations were carried out to further analyze the TGA molecule and its properties.

4.2 Computational Details

All calculations were conducted using the Gaussian 16 suite of programs. Geometry optimization was performed at the CCSD/cc-pVDZ level of theory. To generate potential energy surfaces, a relaxed scan was carried out at the CCSD/cc-pVDZ level of theory with a step size of 5° variations in all dihedral angles, namely S5-C1-C4-O8, H6-S5-C1-C4, and H9-O8-C4-C1 (atom numbering as per Figure 4.3). Single point

calculations were performed at the CCSD(T) level of theory using cc-pVNZ basis sets (where N = T, Q) for all TGA monomers, dimers, and trimers. The Helgaker method was applied to extrapolate the correlation energy, and results were obtained using cc-pVNZ basis sets (where N = T, Q).

Geometrical parameters were calculated and the charges were analyzed using the same level of theory (CCSD/cc-pVDZ). To explore S-centered H-bonding dimers and trimers of most stable conformer of TGA were studied at CCSD/cc-pVDZ theoretical level. Harmonic vibrational IR active modes were calculated for all monomers, dimers and trimers clusters of TGA at the B3LYP/cc-pVTZ//CCSD/cc-pVDZ level of theory and assigned by visualizing the modes using the Gauss view 6.0.1 platform. Here, B3LYP/cc-pVTZ//CCSD/cc-pVDZ means that first these systems optimized at CCSD/cc-pVDZ level then these optimized geometries were used for frequency calculation at B3LYP/cc-pVTZ level of theory. Because the frequency results were best reproduced at B3LYP/cc-pVTZ level of theory. Electrostatic potential (ESP) mapping was conducted on the optimized structures of TGA clusters to identify potential reactive centers. The intramolecular and intermolecular (H-bond) interactions were investigated using AIM calculations, RDG analysis, and visualization through the Multiwfn software. Furthermore, the NBO calculation was employed to investigate intra and inter molecular charge transfer, hyperconjugative interactions, and their strengths in TGA monomers, dimers, and trimers. The FMO calculation provided insights into the chemical reactivity and stability of the systems. Based on the FMO results, the global reactivity descriptors such as μ, η, χ, and ω (Electrophilicity index) were calculated using the equations mentioned in introduction section 1.6.6.

Also, the application of Domain-based Local Pair Natural Orbitals Coupled-Cluster theory incorporating single, double, and perturbative triple excitations (DLPNO-CCSD(T)) has been employed for LED (Local Energy Decomposition) calculation. This approach yields outcomes that closely approach those of its parent CCSD(T) method and by employing the Normal Pair Natural Orbitals truncation threshold, one can come close to the CCSD(T) results within a range of 1 kcal/mol.[32] The DLPNO-CCSD(T) approach

offers accuracy that approaches its parent canonical CCSD(T) method, widely regarded as the benchmark standard. However, DLPNO-CCSD(T) maintains computational efficiency unlike CCSD(T), and it exhibits linear scalability with contemporary DFT methods.[32] The Local Energy Decomposition (LED) technique dissects the energies of DLPNO-CCSD(T) into significant physical components originating from the fragments. These components encompass electrostatic energy, electron exchange energy, London dispersion elements, and other pivotal contributions.[33] Thus, in this chapter, LED analysis has additionally been carried out to delve into the interactions occurring within TGA clusters, spanning across both dimers and trimers.

4.3 Results and Discussion

4.3.1 Conformational Analysis

The conformational space of TGA was explored at the CCSD/cc-pVDZ level of theory using a relaxed scan approach as mentioned in the computational details section. In the relaxed scan of the H6-S5-C1-C4 dihedral angle (Figure 4.1a), a global minimum conformation called GGC was observed, followed by a conformer named GAC, which is 0.16 kcal/mol higher in energy than the global minimum. Similarly, in the relaxed scan of the S5-C1-C4-O8 dihedral angle, the same two conformers (GGC and GAC) were observed, with GGC being the most stable one. However, in the relaxed scan of the H9-O8-C4-C1 dihedral angle, only the GGC conformer was observed as the most stable conformer although the local minimum conformer, GAT, was found at much higher energy (-6.18 kcal/mol) with respect to the GGC conformer. Therefore, this higher energy conformer was not chosen for detailed computational analysis though the optimized structure of GAT conformer is shown in figure 4.4. The same results were obtained when these dihedral angles were scanned (relaxed) at CCSD/cc-pVTZ level of theory, shown in figure 4.2. To explore the possibility of additional stable conformers, a simultaneous dihedral relaxed scan was performed by rotating both the S5-C1 and C1-C4 bonds (figure 4.1(d)). And This 2D relaxed scan confirmed the GGC conformation as the global minimum.

The nomenclature of the conformers of TGA monomers used in this study follows the nomenclature established by Reva D. et al. for glycolic acid.[34] Briefly, the conformers were assigned labels consisting of three capital letters, representing the orientations of the following dihedral angles: H6-S5-C1-C4, S5-C1-C4-O7, and O7-C4-O8-H9 (the numbers after the atomic symbols follow the labeling scheme shown in Figure 4.3). The letters used for labeling were G (gauche), A (anti), and C (cis).

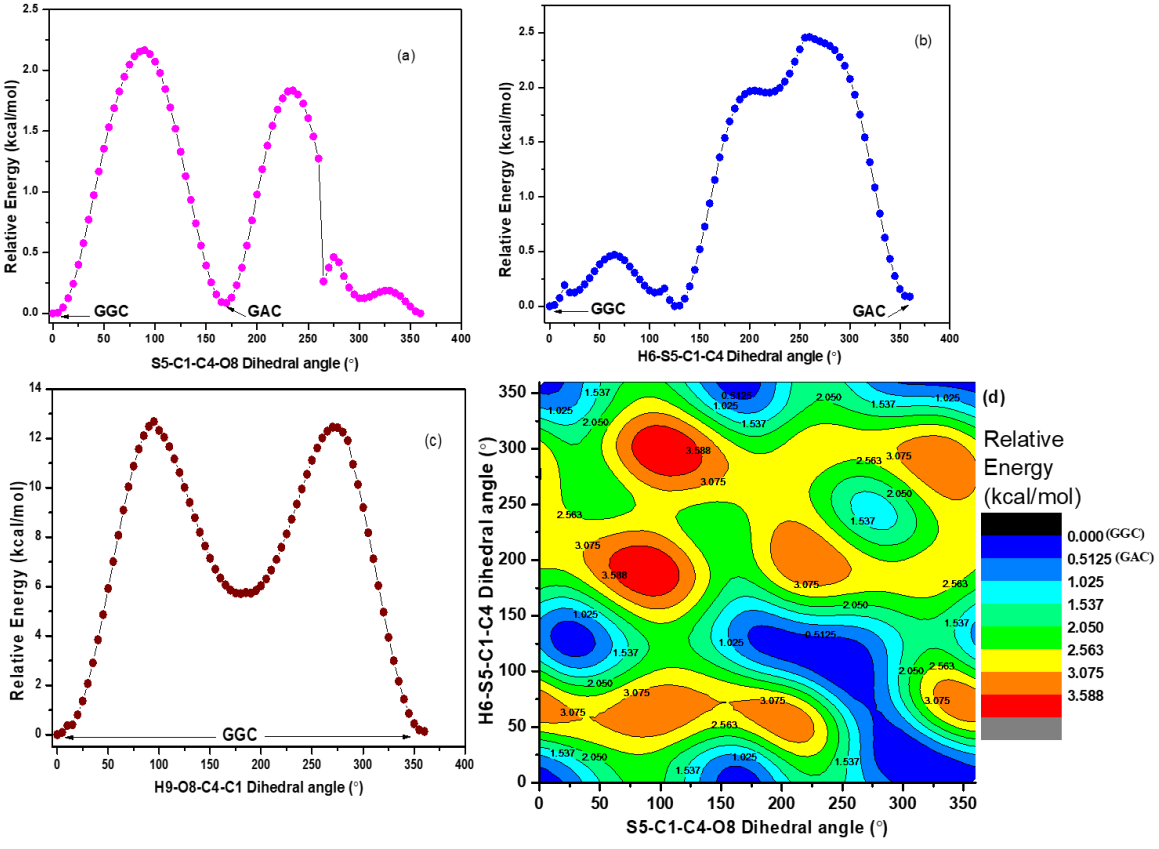

Figure 4.1: Potential energy curve [a (C1-C4 bond rotation) and b (S5-C1 bond rotation) c (O8-C4 bond rotation)] and Potential energy surface (d) for simultaneous rotation of C1-C4 and S5-C1 bond of TGA generated at CCSD/cc-pVDZ level of theory. (Number after the atomic symbol represents the labeling scheme as per Figure 4.3).

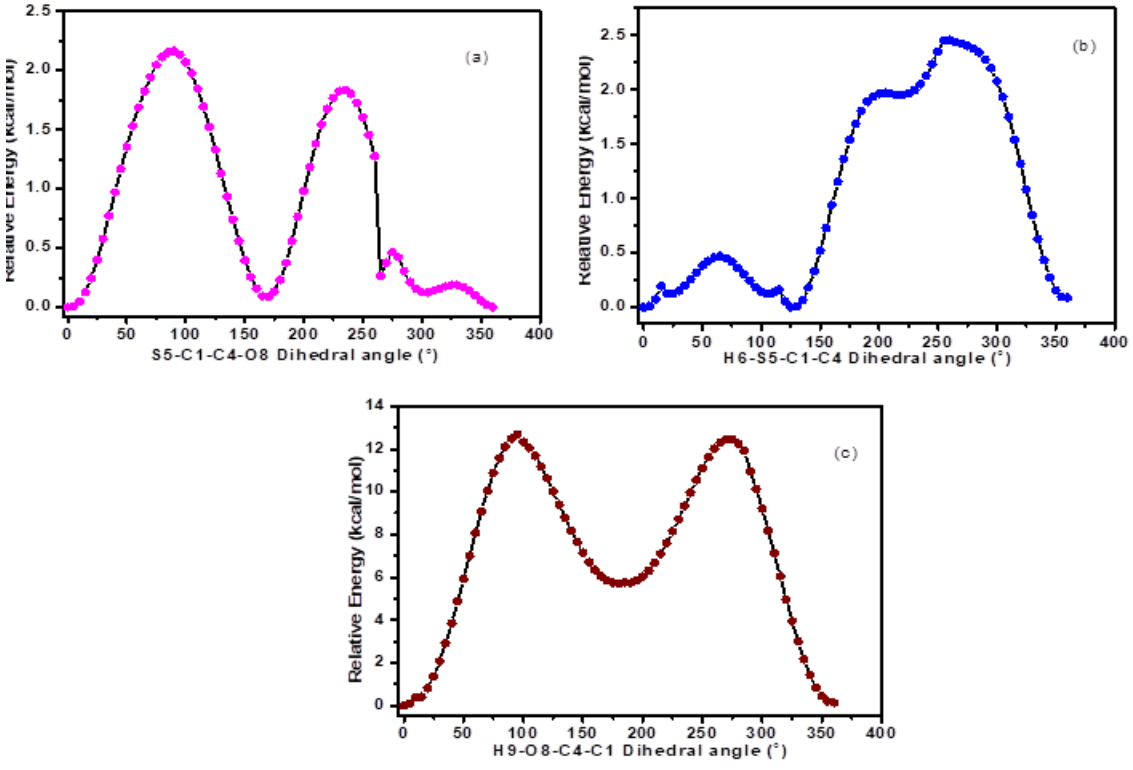

Figure 4.2: Potential energy curve [a (C1-C4 bond rotation) and b (S5-C1 bond rotation) c (O8-C4 bond rotation)] of TGA generated at CCSD/cc-pVTZ level of theory. (Number after the atomic symbol represents the labeling scheme as per Figure 4.3).

Barrier Height Calculation:

In the experimental study (microwave spectroscopy) conducted by Yamaguchi et al.[35] it was suggested that the barrier for S-H flipping in TGA is low although explicit rotational barrier value was not provided. In comparison, in past studies the calculated barriers for O-H flipping in propargyl alcohol, internal rotation in methyl mercaptane, and methanol were found to be 0.25 kcal/mol, 1.27 kcal/mol, and 1.07 kcal/mol, respectively.[36–38] Fantoni et al. reported a SH flipping barrier of 0.22 kcal/mol at the B3LYP/6-31+G**//B3LYP/6-31G** level of theory and 0.07 kcal/mol at MP2/cc-pVTZ//MP2/6-31G** in TGA.[39] In the present study, the barrier for S-H flipping was observed to be 1.9 kcal/mol [in case of C-C bond rotation] and 2.8 kcal/mol [in case of C-S bond rotation] at the CCSD/cc-pVDZ level of theory which although are higher

compared to the values reported by Fantoni et al. are yet low in terms of absolute values. Consequently, the interconversion of these two conformers can be considered highly spontaneous due to the low energy barrier.

The TGA conformers GGC and GAC were further optimized at the CCSD/cc-pVDZ level of theory (shown in figure 4.3), and their rotational constants with vibrational contribution were calculated at the same level. Notably, the calculated rotational constants for conformer GGC exhibit a favorable agreement with experimental data,[18] albeit with a slight disparity in the A constant even when vibrational contributions are accounted for. Notably, at this specific calculation level, the A constant aligns more closely with experimental values compared to other methods where the discrepancy is greater. Conversely, the computed rotational constants for conformer GAC do not align with experimental data, indicating that the experimental observation was likely limited to the GGC conformer. The calculated rotational constants are provided in the table 4.4a alongside the calculated geometrical parameters of the TGA conformers.

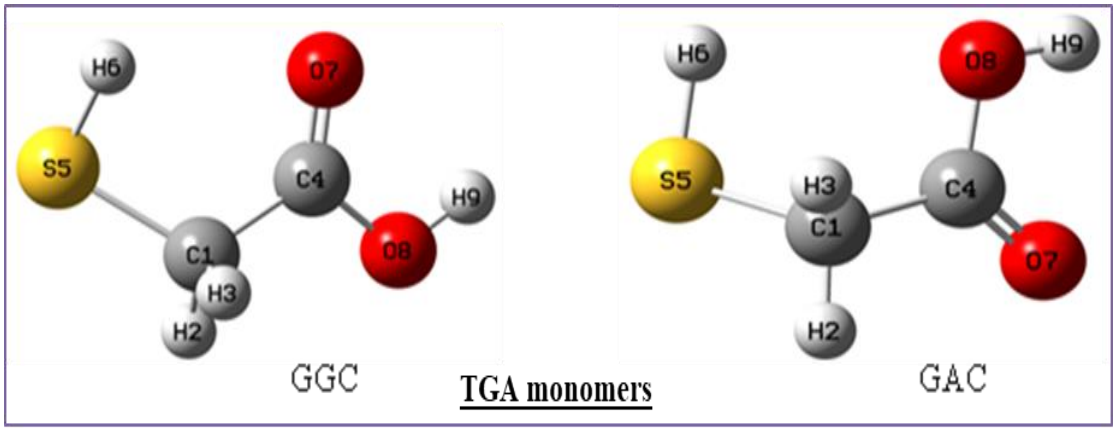

Figure 4.3: Optimized structures of both the TGA monomers (GGC & GAC) at CCSD/cc-pVDZ level; where, numbers after atoms represent the label of that atom in optimized geometry

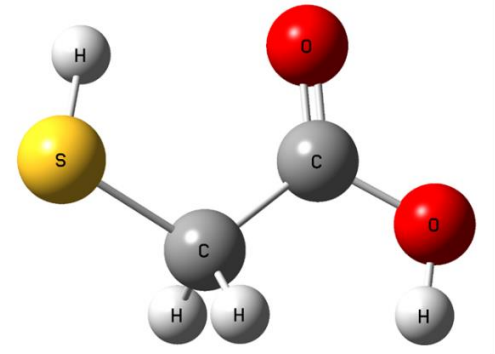

GAT (-6.18 kcal/mol higher in energy than GGC conformer

Figure 4.4: Optimized structure of GAT High energy conformer at CCSD/cc-pVDZ theoretical level

The CCSD(T)/CBS level of theory is widely recognized as the gold standard for studying non-covalent interactions in molecules.[40–42] However, due to its high computational cost, only single-point energy calculations for the TGA conformers using the cc-pVNZ basis set (N = T, Q) with a CBS limit was carried out. The energy values obtained at this level, shown in table 4.1, confirmed the same energy order observed between the two TGA conformers at the CCSD/cc-pVDZ level. Hence, the relative energies of the conformers remained consistent even at the CCSD/CBS limit.

Table 4.1: Relative single point energy difference (CBS limit) with respect to GGC conformer (kcal/mol) at CCSD(T)/ (cc-pVNZ, N=T, Q) level

CBS limit (cc-pVNZ, N=T,Q)	GAC
HF	2.0
MP2	0.8
MP3	1.1
MP4D	0.8
CCSD	0.9
CCSD(T)	0.6

The TGA molecule contains both a carboxylic group and an SH group, suggesting the possibility of intermolecular hydrogen bond interactions involving both

oxygen and sulfur moieties. To investigate sulfur-centered hydrogen bonding, dimers and trimers of TGA were examined. The dimers were constructed using only the global minimum GGC conformer. Various orientations for TGA dimers were designed and optimized at the CCSD/cc-pVDZ level of theory, shown in figure 4.5. Among these dimers, five stable clusters named D1, D2, D3, D4, and D5 were identified. And their Interaction energies were determined by taking the difference between the cluster's energy and the combined energies of the isolated molecules, employing the supermolecule methodology.[43,44] This process is recognized to be susceptible to a significant error known as the Basis Set Superposition Error (BSSE).[43–45] To mitigate this issue, the interaction energies were computed using the counterpoise method introduced by Boys and Bernardi.[46] This technique involves utilizing the basis set of the entire cluster to calculate energies:

$$\Delta E_{ij\ldots} = E_{ij\ldots}(ij\ldots) - \sum_i E_i(ij\ldots) \qquad (1)$$

The BSSE corrected interaction energy for each dimer cluster are depicted in table 4.2. The results show that D1 dimer was the most stable, with an interaction energy of -14.64 kcal/mol.

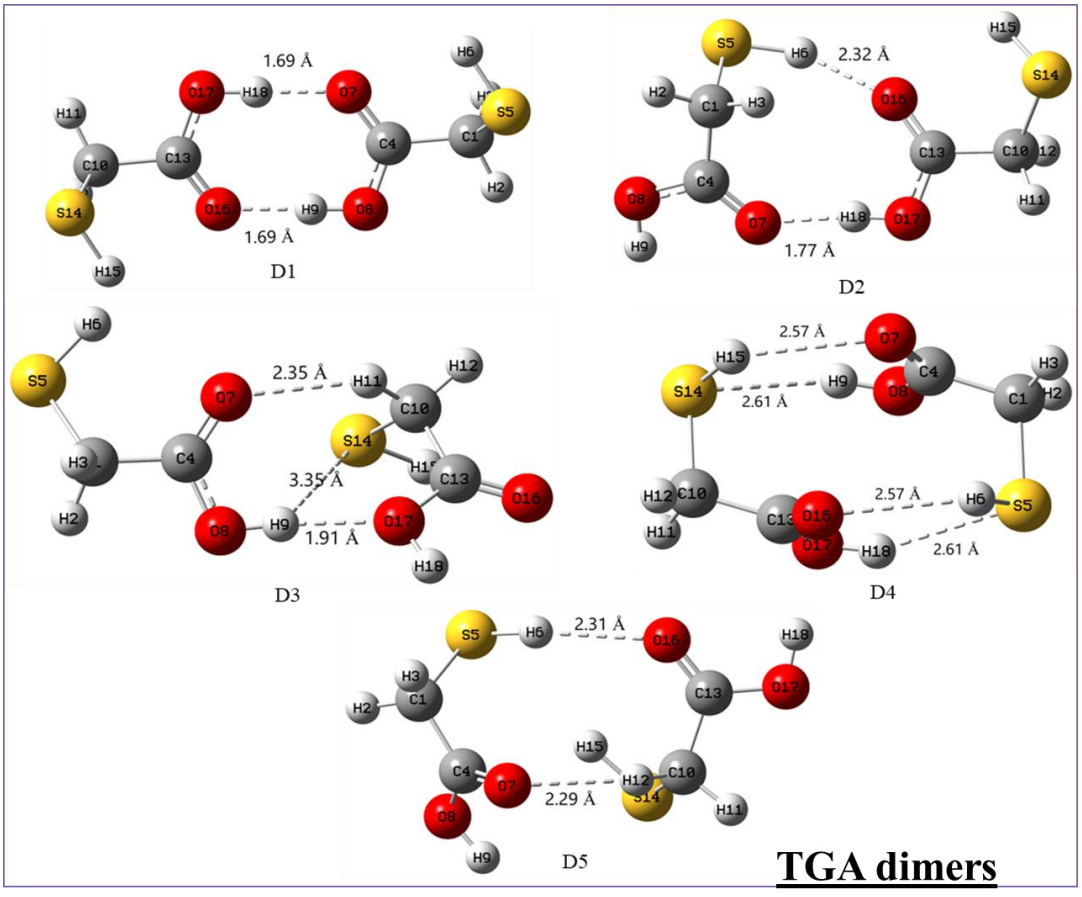

Figure 4.5: Optimized structures of both the TGA dimers (D1-D5) at CCSD/cc-pVDZ level; where, numbers after atoms represent the label of that atom in optimized geometry

Table 4.2: Calculated Interaction Energy of TGA(GGC) Dimers at CCSD/cc-PVDZ level of theory

Dimers of GGC conformers	BSSE corrected Interaction Energy(kcal/mol)
D1	-14.64
D2	-8.90
D3	-5.31
D4	-4.79
D5	-3.59

Similarly, trimer clusters of TGA were constructed by using D1 as the basic unit and orienting the third TGA molecule in different ways to cover all possible

intermolecular interactions. These trimers were then optimized at the CCSD/cc-pVDZ level of theory, shown in figure 4.6. Among the seven stable trimers named T1, T2, T3, T4, T5, T6, and T7, T1 was found to be the global minimum with a BSSE-corrected interaction energy of -22.87 kcal/mol, as shown in table 4.3. For trimers also, similar to dimers, the interaction energies were obtained using the counterpoise method of Boys and Bernardi.[46] The calculated geometrical parameters of TGA monomers, dimers, and trimers are shown in table 4.4a, 4.4b and 4.4c.

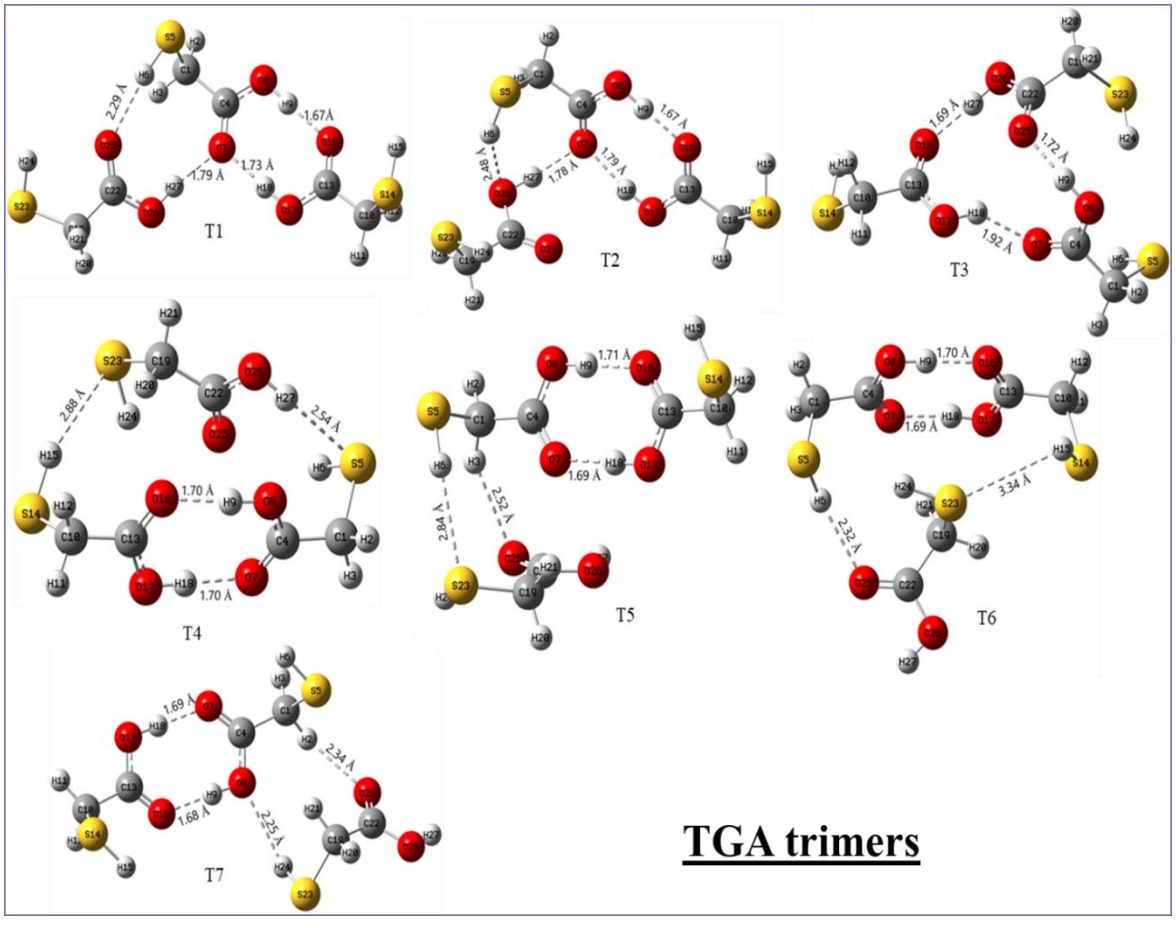

Figure 4.6: Optimized structures of all 7 trimers (T1-T7) of TGA at CCSD/cc-pVDZ level; where, numbers after atoms represent the label of that atom in optimized geometry

Table 4.3: Calculated Interaction Energy of TGA(GGC) Trimers at CCSD/cc-PVDZ level of theory

Trimer Systems	BSSE Corrected Interaction Energy (kcal/mol)
T1	-22.87
T2	-19.92
T3	-19.37
T4	-19.2
T5	-17.74
T6	-17.57
T7	-17.48

Table 4.4a: Optimized geometries, rotational constants (MHz) [A, B, C], inertia defect (amu. $Å^2$ [Δ_C] of TGA monomers (GGC and GAC) at CCSD/cc-pVDZ level of theory (R is distance in Å, Θ is angle in degree (°). Values in the paraenthsis in the first column are the experimental values from Reference 18.

Geometrical parameters	**GGC**	**GAC**
R_{S-H}	1.35	1.35
R_{S-C}	1.82	1.83
R_{C-H}	1.10	1.10
	1.10	1.10
R_{O-H}	0.97	0.97
R_{C-C}	1.52	1.51
R_{C-O}	1.35	1.35
$R_{C=O}$	1.21	1.21
Θ_{C-S-H}	94.6	95.3
Θ_{H-O-C}	105.4	105.4
$\Theta_{C-C-S-H}$	-42.8	-64.5
$\Theta_{H-O-C=O}$	0.75	1.62
$\Theta_{S-C-C=O}$	29.9	-111.1
A (10028.5)	9745.5	8253.3
B (2346.0)	2324.6	2452.7
C (1951.7)	1945.1	2143.5
Δ_C (-6.87)	-9.44	-31.51

Table 4.4b: Optimized geometrical parameters of dimers of TGA at CCSD/cc-pVDZ (R is distance in Å, Θ is angle in degree (°)

Geometrical parameters	**GGC**	**D1**	**D2**	**D3**	**D4**	**D5**
R_{S-H}	1.35	R_{S5-H} = 1.35	R_{S5-H} = 1.35	R_{S5-H} = 1.35	R_{S5-H} = 1.35	R_{S5-H} = 1.35
		R_{S14-H} = 1.35	R_{S14-H} = 1.35	R_{S14-H} = 1.35	R_{S14-H} = 1.35	R_{S14-H} = 1.35
R_{S-C}	1.82	R_{S5-C1} = 1.83	R_{S5-C1} = 1.84	R_{S5-C1} = 1.82	R_{S5-C1} = 1.84	R_{S5-C1} = 1.84
		$R_{S14-C10}$ = 1.83	$R_{S14-C10}$ = 1.83	$R_{S14-C10}$ = 1.83	$R_{S14-C10}$ = 1.84	$R_{S14-C10}$ = 1.84
R_{C-H}	1.10	R_{C1-H2} = 1.10	R_{C1-H2} = 1.10	R_{C1-H2} = 1.10	R_{C1-H2} = 1.10	R_{C1-H2} = 1.10
		R_{C1-H3} = 1.10	R_{C1-H3} = 1.09	R_{C1-H3} = 1.10	R_{C1-H3} = 1.10	R_{C1-H3} = 1.10
	1.10	$R_{C10-H11}$ = 1.10	$R_{C10-H11}$ = 1.10	$R_{C10-H11}$ = 1.10	$R_{C10-H11}$ = 1.10	$R_{C10-H11}$ = 1.10
		$R_{C10-H12}$ = 1.10	$R_{C10-H12}$ = 1.10	$R_{C10-H12}$ = 1.09	$R_{C10-H12}$ = 1.10	$R_{C10-H12}$ = 1.09
R_{O-H}	0.97	R_{O8-H9} = 0.99	R_{O8-H9} = 0.97	R_{O8-H9} = 0.98	R_{O8-H9} = 0.97	R_{O8-H9} = 0.97
		$R_{O17-H18}$ = 0.99	$R_{O17-H18}$ = 0.98	$R_{O17-H18}$ = 0.97	$R_{O17-H18}$ = 0.97	$R_{O17-H18}$ = 0.97
R_{C-C}	1.52	R_{C1-C4} = 1.51	R_{C1-C4} = 1.51	R_{C1-C4} = 1.52	R_{C1-C4} = 1.51	R_{C1-C4} = 1.51
		$R_{C10-C13}$ = 1.51	$R_{C10-C13}$ = 1.52	$R_{C10-C13}$ = 1.51	$R_{C10-C13}$ = 1.51	$R_{C10-C13}$ = 1.51
R_{C-O}	1.35	R_{C4-O8} = 1.32	R_{C4-O8} = 1.34	R_{C4-O8} = 1.34	R_{C4-O8} = 1.34	R_{C4-O8} = 1.35
		$R_{C13-O17}$ = 1.32	$R_{C13-O17}$ = 1.33	$R_{C13-O17}$ = 1.37	$R_{C13-O17}$ = 1.34	$R_{C13-O17}$ = 1.35
$R_{C=O}$	1.21	$R_{C4=O7}$ = 1.22	$R_{C4=O7}$ = 1.22	$R_{C4=O7}$ = 1.21	$R_{C4=O7}$ = 1.21	$R_{C4=O7}$ = 1.21
		$R_{C13=O16}$ = 1.22	$R_{C13=O16}$ = 1.21	$R_{C13=O16}$ = 1.20	$R_{C13=O16}$ = 1.21	$R_{C13=O16}$ = 1.21
Θ_{C-S-H}	94.6	$\Theta_{C1-S5-H6}$ = 94.6	$\Theta_{C1-S5-H6}$ = 94.0	$\Theta_{C1-S5-H6}$ = 94.6	$\Theta_{C1-S5-H6}$ = 95.6	$\Theta_{C1-S5-H6}$ = 96.0
		$\Theta_{C10-S14-H15}$ = 94.6	$\Theta_{C10-S14-H15}$ = 94.6	$\Theta_{C10-S14-H15}$ = 95.4	$\Theta_{C10-S14-H15}$ = 95.6	$\Theta_{C10-S14-H15}$ = 95.6
Θ_{H-O-C}	105.4	$\Theta_{H9-O8-C4}$ = 108.6	$\Theta_{H9-O8-C4}$ = 105.8	$\Theta_{H9-O8-C4}$ = 107.2	$\Theta_{H9-O8-C4}$ = 106.9	$\Theta_{H9-O8-C4}$ = 105.7
		$\Theta_{H18-O17-C13}$ = 108.6	$\Theta_{H18-O17-C13}$ = 107.9	$\Theta_{H18-O17-C13}$ = 105.6	$\Theta_{H18-O17-C13}$ = 107.0	$\Theta_{H18-O17-C13}$ = 105.5

$\Theta_{C\text{-}C\text{-}S\text{-}H}$	-42.8	$\Theta_{C4\text{-}C1\text{-}S5\text{-}H6}$ = -58.7	$\Theta_{C4\text{-}C1\text{-}S5\text{-}H6}$ = -83.8	$\Theta_{C4\text{-}C1\text{-}S5\text{-}H6}$ = -42.2	$\Theta_{C4\text{-}C1\text{-}S5\text{-}H6}$ = -57.7	$\Theta_{C4\text{-}C1\text{-}S5\text{-}H6}$ = -60.4
		$\Theta_{C13\text{-}C10\text{-}S14\text{-}H15}$ = -58.7	$\Theta_{C13\text{-}C10\text{-}S14\text{-}H15}$ = -43.9	$\Theta_{C13\text{-}C10\text{-}S14\text{-}H15}$ = -64.4	$\Theta_{C13\text{-}C10\text{-}S14\text{-}H15}$ = -57.8	$\Theta_{C13\text{-}C10\text{-}S14\text{-}H15}$ = -60.6
$\Theta_{H\text{-}O\text{-}C=O}$	0.75	$\Theta_{H9\text{-}O8\text{-}C4=O7}$ = -0.87	$\Theta_{H9\text{-}O8\text{-}C4=O7}$ = -2.24	$\Theta_{H9\text{-}O8\text{-}C4=O7}$ = 1.0	$\Theta_{H9\text{-}O8\text{-}C4=O7}$ = -8.3	$\Theta_{H9\text{-}O8\text{-}C4=O7}$ = -5.3
		$\Theta_{H18\text{-}O17\text{-}C13=O16}$ = -0.87	$\Theta_{H18\text{-}O17\text{-}C13=O16}$ = 1.09	$\Theta_{H18\text{-}O17\text{-}C13=O16}$ = -1.7	$\Theta_{H18\text{-}O17\text{-}C13=O16}$ = -8.3	$\Theta_{H18\text{-}O17\text{-}C13=O16}$ = -1.3
$\Theta_{S\text{-}C\text{-}C=O}$		$\Theta_{S5\text{-}C1\text{-}C4=O7}$ = 68.7	$\Theta_{S5\text{-}C1\text{-}C4=O7}$ = 92.0	$\Theta_{S5\text{-}C1\text{-}C4=O7}$ = 30.1	$\Theta_{S5\text{-}C1\text{-}C4=O7}$ = 97.3	$\Theta_{S5\text{-}C1\text{-}C4=O7}$ = 94.2
		$\Theta_{S14\text{-}C10\text{-}C13=O16}$ = 68.7	$\Theta_{S14\text{-}C10\text{-}C13=O16}$ = 33.1	$\Theta_{S14\text{-}C10\text{-}C13=O16}$ = 100.9	$\Theta_{S14\text{-}C10\text{-}C13=O16}$ = 97.3	$\Theta_{S14\text{-}C10\text{-}C13=O16}$ = 79.6

Table 4.4c: Optimized geometrical parameters of trimers of TGA at CCSD/cc-pVDZ (R is distance in Å, Θ is angle in degree (°)

Geometrical parameters	**GGC**	**T1**	**T2**	**T3**	**T4**	**T5**	**T6**	**T7**
$R_{S\text{-}H}$	1.35	$R_{S5\text{-}H}$ = 1.35	$R_{S5\text{-}H}$ = 1.35	$R_{S5\text{-}H}$ = 1.35	$R_{S5\text{-}H}$ = 1.35	$R_{S5\text{-}H}$ = 1.35	$R_{S5\text{-}H}$ = 1.35	$R_{S5\text{-}H}$ = 1.35
		$R_{S14\text{-}H}$ = 1.35	$R_{S14\text{-}H}$ = 1.35	$R_{S14\text{-}H}$ = 1.35	$R_{S14\text{-}H}$ = 1.35	$R_{S14\text{-}H}$ = 1.35	$R_{S14\text{-}H}$ = 1.35	$R_{S14\text{-}H}$ = 1.35
		$R_{S23\text{-}H}$ = 1.35	$R_{S23\text{-}H}$ = 1.35	$R_{S23\text{-}H}$ = 1.35	$R_{S23\text{-}H}$ = 1.35	$R_{S23\text{-}H}$ = 1.35	$R_{S23\text{-}H}$ = 1.35	$R_{S23\text{-}H}$ = 1.35
$R_{S\text{-}C}$	1.82	$R_{S5\text{-}C1}$ = 1.84	$R_{S5\text{-}C1}$ = 1.84	$R_{S5\text{-}C1}$ = 1.84	$R_{S5\text{-}C1}$ = 1.84	$R_{S5\text{-}C1}$ = 1.84	$R_{S5\text{-}C1}$ = 1.84	$R_{S5\text{-}C1}$ = 1.84
		$R_{S14\text{-}C10}$ = 1.83	$R_{S14\text{-}C10}$ = 1.83	$R_{S14\text{-}C10}$ = 1.83	$R_{S14\text{-}C10}$ = 1.83	$R_{S14\text{-}C10}$ = 1.83	$R_{S14\text{-}C10}$ = 1.84	$R_{S14\text{-}C10}$ = 1.83
		$R_{S23\text{-}C19}$ = 1.83	$R_{S23\text{-}C19}$ = 1.84	$R_{S23\text{-}C19}$ = 1.84	$R_{S23\text{-}C19}$ = 1.83	$R_{S23\text{-}C19}$ = 1.82	$R_{S23\text{-}C19}$ = 1.84	$R_{S23\text{-}C19}$ = 1.84
$R_{C\text{-}H}$	1.10	$R_{C1\text{-}H2}$ = 1.10	$R_{C1\text{-}H2}$ = 1.10	$R_{C1\text{-}H2}$ = 1.10	$R_{C1\text{-}H2}$ = 1.10	$R_{C1\text{-}H2}$ = 1.10	$R_{C1\text{-}H2}$ = 1.10	$R_{C1\text{-}H2}$ = 1.09
		$R_{C10\text{-}H11}$ = 1.10	$R_{C10\text{-}H11}$ = 1.10	$R_{C10\text{-}H11}$ = 1.10	$R_{C10\text{-}H11}$ = 1.10	$R_{C10\text{-}H11}$ = 1.10	$R_{C10\text{-}H11}$ = 1.10	$R_{C10\text{-}H11}$ = 1.10
		$R_{C19\text{-}H20}$ = 1.10	$R_{C19\text{-}H20}$ = 1.10	$R_{C19\text{-}H20}$ = 1.10	$R_{C19\text{-}H20}$ = 1.10	$R_{C19\text{-}H20}$ = 1.10	$R_{C19\text{-}H20}$ = 1.10	$R_{C19\text{-}H20}$ = 1.10
	1.10	$R_{C1\text{-}H3}$ = 1.09	$R_{C1\text{-}H3}$ = 1.10	$R_{C1\text{-}H3}$ = 1.10	$R_{C1\text{-}H3}$ = 1.09	$R_{C1\text{-}H3}$ = 1.09	$R_{C1\text{-}H3}$ = 1.09	$R_{C1\text{-}H3}$ = 1.09

		$R_{C10-H12}$ = 1.10	$R_{C10-H12}$ = 1.10	$R_{C10-H12}$ = 1.10	$R_{C10-H12}$ = 1.10	$R_{C10-H12}$ = 1.10	$R_{C10-H12}$ = 1.10	$R_{C10-H12}$ = 1.10
		$R_{C19-H21}$ = 1.10	$R_{C19-H21}$ = 1.10	$R_{C19-H21}$ = 1.10	$R_{C19-H21}$ = 1.10	$R_{C19-H21}$ = 1.10	$R_{C19-H21}$ = 1.09	$R_{C19-H21}$ = 1.09
R_{O-H}	0.97	R_{O8-H9} = 0.99	R_{O8-H9} = 0.99	R_{O8-H9} = 0.99	R_{O8-H9} = 0.99	R_{O8-H9} = 0.99	R_{O8-H9} = 0.99	R_{O8-H9} = 0.99
		$R_{O17-H18}$ = 0.99	$R_{O17-H18}$ = 0.98	$R_{O17-H18}$ = 0.98	$R_{O17-H18}$ = 0.99	$R_{O17-H18}$ = 0.99	$R_{O17-H18}$ = 0.99	$R_{O17-H18}$ = 0.99
		$R_{O26-H27}$ = 0.98	$R_{O26-H27}$ = 0.98	$R_{O26-H27}$ = 0.99	$R_{O26-H27}$ = 0.98	$R_{O26-H27}$ = 0.97	$R_{O26-H27}$ = 0.97	$R_{O26-H27}$ = 0.97
R_{C-C}	1.52	R_{C1-C4} = 1.51	R_{C1-C4} = 1.51	R_{C1-C4} = 1.51	R_{C1-C4} = 1.51	R_{C1-C4} = 1.51	R_{C1-C4} = 1.51	R_{C1-C4} = 1.51
		$R_{C10-C13}$ = 1.51	$R_{C10-C13}$ = 1.52	$R_{C10-C13}$ = 1.52	$R_{C10-C13}$ = 1.51	$R_{C10-C13}$ = 1.51	$R_{C10-C13}$ = 1.51	$R_{C10-C13}$ = 1.51
		$R_{C19-C22}$ = 1.52	$R_{C19-C22}$ = 1.51	$R_{C19-C22}$ = 1.51	$R_{C19-C22}$ = 1.52	$R_{C19-C22}$ = 1.52	$R_{C19-C22}$ = 1.51	$R_{C19-C22}$ = 1.51
R_{C-O}	1.35	R_{C4-O8} = 1.31	R_{C4-O8} = 1.31	R_{C4-O8} = 1.33	R_{C4-O8} = 1.31	R_{C4-O8} = 1.32	R_{C4-O8} = 1.32	R_{C4-O8} = 1.32
		$R_{C13-O17}$ = 1.32	$R_{C13-O17}$ = 1.32	$R_{C13-O17}$ = 1.32	$R_{C13-O17}$ = 1.32	$R_{C13-O17}$ = 1.32	$R_{C13-O17}$ = 1.32	$R_{C13-O17}$ = 1.32
		$R_{C22-O26}$ = 1.33	$R_{C22-O26}$ = 1.34	$R_{C22-O26}$ = 1.32	$R_{C22-O26}$ = 1.33	$R_{C22-O26}$ = 1.35	$R_{C22-O26}$ = 1.34	$R_{C22-O26}$ = 1.35
$R_{C=O}$	1.21	$R_{C4=O7}$ = 1.23	$R_{C4=O7}$ = 1.23	$R_{C4=O7}$ = 1.22	$R_{C4=O7}$ = 1.23	$R_{C4=O7}$ = 1.23	$R_{C4=O7}$ = 1.23	$R_{C4=O7}$ = 1.22
		$R_{C13=O16}$ = 1.22	$R_{C13=O16}$ = 1.22	$R_{C13=O16}$ = 1.22	$R_{C13=O16}$ = 1.22	$R_{C13=O16}$ = 1.22	$R_{C13=O16}$ = 1.22	$R_{C13=O16}$ = 1.22
		$R_{C22=O25}$ = 1.21	$R_{C22=O25}$ = 1.21	$R_{C22=O25}$ = 1.22	$R_{C22=O25}$ = 1.21	$R_{C22=O25}$ = 1.21	$R_{C22=O25}$ = 1.21	$R_{C22=O25}$ = 1.21
Θ_{C-S-H}	94.6	$\Theta_{C1-S5-H6}$ = 94.1	$\Theta_{C1-S5-H6}$ = 95.7	$\Theta_{C1-S5-H6}$ = 95.1	$\Theta_{C1-S5-H6}$ = 95.7	$\Theta_{C1-S5-H6}$ = 94.5	$\Theta_{C1-S5-H6}$ = 96.6	$\Theta_{C1-S5-H6}$ = 95.2
		$\Theta_{C10-S14-H15}$ = 94.8	$\Theta_{C10-S14-H15}$ = 94.8	$\Theta_{C10-S14-H15}$ = 94.6	$\Theta_{C10-S14-H15}$ = 96.2	$\Theta_{C10-S14-H15}$ = 94.7	$\Theta_{C10-S14-H15}$ = 95.3	$\Theta_{C10-S14-H15}$ = 94.7
		$\Theta_{C19-S23-H24}$ = 94.6	$\Theta_{C19-S23-H24}$ = 95.1	$\Theta_{C19-S23-H24}$ = 95.9	$\Theta_{C19-S23-H24}$ = 94.4	$\Theta_{C19-S23-H24}$ = 95.2	$\Theta_{C19-S23-H24}$ = 95.8	$\Theta_{C19-S23-H24}$ = 94.6
Θ_{H-O-C}	105.4	$\Theta_{H9-O8-C4}$ = 109.5	$\Theta_{H9-O8-C4}$ = 108.7	$\Theta_{H9-O8-C4}$ = 107.2	$\Theta_{H9-O8-C4}$ = 108.4	$\Theta_{H9-O8-C4}$ = 108.6	$\Theta_{H9-O8-C4}$ = 108.8	$\Theta_{H9-O8-C4}$ = 108.6
		$\Theta_{H18-O17-C13}$ = 108.2	$\Theta_{H18-O17-C13}$ = 108.9	$\Theta_{H18-O17-C13}$ = 111.1	$\Theta_{H18-O17-C13}$ = 108.9	$\Theta_{H18-O17-C13}$ = 108.3	$\Theta_{H18-O17-C13}$ = 108.2	$\Theta_{H18-O17-C13}$ = 108.6
		$\Theta_{H27-O26-C22}$ = 107.8	$\Theta_{H27-O26-C22}$ = 106.3	$\Theta_{H27-O26-C22}$ = 107.4	$\Theta_{H27-O26-C22}$ = 106.8	$\Theta_{H27-O26-C22}$ = 105.4	$\Theta_{H27-O26-C22}$ = 105.5	$\Theta_{H27-O26-C22}$ = 105.4
$\Theta_{C-C-S-H}$	-42.8	$\Theta_{C4-C1-S5-H6}$ = -86.3	$\Theta_{C4-C1-S5-H6}$ = -74.4	$\Theta_{C4-C1-S5-H6}$ = -62.3	$\Theta_{C4-C1-S5-H6}$ = -55.9	$\Theta_{C4-C1-S5-H6}$ = -75.3	$\Theta_{C4-C1-S5-H6}$ = -66.3	$\Theta_{C4-C1-S5-H6}$ = -60.8

		$\Theta_{C13-C10-S14-H15}$ = -61.3	$\Theta_{C13-C10-S14-H15}$ = -50.3	$\Theta_{C13-C10-S14-H15}$ = -56.5	$\Theta_{C13-C10-S14-H15}$ = -67.8	$\Theta_{C13-C10-S14-H15}$ = -60.1	$\Theta_{C13-C10-S14-H15}$ = -61.5	$\Theta_{C13-C10-S14-H15}$ = -58.9
		$\Theta_{C22-C19-S23-H24}$ = -44.5	$\Theta_{C22-C19-S23-H24}$ = -62.9	$\Theta_{C22-C19-S23-H24}$ = -69.5	$\Theta_{C22-C19-S23-H24}$ = 34.0	$\Theta_{C22-C19-S23-H24}$ = 35.3	$\Theta_{C22-C19-S23-H24}$ = -66.1	$\Theta_{C22-C19-S23-H24}$ = -74.7
$\Theta_{H-O-C=O}$	0.75	$\Theta_{H9-O8-C4=O7}$ = -2.23	$\Theta_{H9-O8-C4=O7}$ = -2.95	$\Theta_{H9-O8-C4=O7}$ = -6.32	$\Theta_{H9-O8-C4=O7}$ = -8.62	$\Theta_{H9-O8-C4=O7}$ = -2.07	$\Theta_{H9-O8-C4=O7}$ = -3.71	$\Theta_{H9-O8-C4=O7}$ = -1.66
		$\Theta_{H18-O17-C13=O16}$ = -1.15	$\Theta_{H18-O17-C13=O16}$ = 0.64	$\Theta_{H18-O17-C13=O16}$ = -2.48	$\Theta_{H18-O17-C13=O16}$ = -4.57	$\Theta_{H18-O17-C13=O16}$ = -2.24	$\Theta_{H18-O17-C13=O16}$ = -3.80	$\Theta_{H18-O17-C13=O16}$ = -0.91
		$\Theta_{H27-O26-C22=O25}$ = 1.69	$\Theta_{H27-O26-C22=O25}$ = -5.75	$\Theta_{H27-O26-C22=O25}$ = -4.21	$\Theta_{H27-O26-C22=O25}$ = -4.82	$\Theta_{H27-O26-C22=O25}$ = 1.86	$\Theta_{H27-O26-C22=O25}$ = -1.73	$\Theta_{H27-O26-C22=O25}$ = -1.65
$\Theta_{S-C-C=O}$		$\Theta_{S5-C1-C4=O7}$ = 91.2	$\Theta_{S5-C1-C4=O7}$ = 87.8	$\Theta_{S5-C1-C4=O7}$ = 90.0	$\Theta_{S5-C1-C4=O7}$ = 114.5	$\Theta_{S5-C1-C4=O7}$ = 87.2	$\Theta_{S5-C1-C4=O7}$ = 93.1	$\Theta_{S5-C1-C4=O7}$ = 84.4
		$\Theta_{S14-C10-C13=O16}$ = 74.9	$\Theta_{S14-C10-C13=O16}$ = 40.4	$\Theta_{S14-C10-C13=O16}$ = 64.3	$\Theta_{S14-C10-C13=O16}$ = 105.4	$\Theta_{S14-C10-C13=O16}$ = 73.9	$\Theta_{S14-C10-C13=O16}$ = 97.7	$\Theta_{S14-C10-C13=O16}$ = 68.7
		$\Theta_{S23-C19-C22=O25}$ = 33.6	$\Theta_{S23-C19-C22=O25}$ = 91.2	$\Theta_{S23-C19-C22=O25}$ = 89.3	$\Theta_{S23-C19-C22=O25}$ = -27.8	$\Theta_{S23-C19-C22=O25}$ = -11.1	$\Theta_{S23-C19-C22=O25}$ = 87.1	$\Theta_{S23-C19-C22=O25}$ = 88.2

Note: Here, numbers after atoms in all these tables represent the label of that particular atom in optimized geometry of TGA monomers, dimers and trimers (Figure 4.2, 4.5 and 4.6).

Single-point energy calculations at the CCSD(T)/CBS limit with the cc-pVNZ basis set (N = T, Q) were also performed for the dimers (Note: Due to infrastructural constraints, such calculations could not be done for the trimers), given in the table 4.5. The energy ordering for the dimer clusters was found to be consistent with that at the CCSD/cc-pVDZ level. Interaction energy for all dimers and trimers calculated at both CCSD/cc-pVDZ and B3LYP/cc-pVTZ level of theory were subjected to ZPE (zero-point energy) correction. And these ZPE corrected + BSSE corrected Interaction energy/Binding energy for all dimers and trimers TGA clusters are provided in table 4.6.

Table 4.5: Relative Single point relative energy difference (CBS limit) with respect to D1 dimer (kcal/mol) at CCSD(T)/cc-pVNZ (N=T, Q) level

Dimers of GGC conformer	CBS limit at HF,MP2, MP3, MP4, CCSD and CCSD(t) method with cc-pVNZ (N=T,Q) basis set					
	HF	MP2	MP3	MP4	CCSD	CCSD(t)
D2	4.42	5.5	5.5	5.3	5.2	5.6
D3	11.5	10.2	11.0	10.2	10.3	6.6
D4	12.6	8.1	10.1	9.0	9.5	8.6
D5	12.8	9.9	11.4	10.5	10.8	10.4

Table 4.6: Calculated ZPE (zero-point energy) + BSSE corrected and only BSSE corrected Interaction energy (kcal/mol) for dimers and trimers clusters of TGA

Dimers (D1-D5) and trimers (T1-T7) of TGA (GGC) conformers	Interaction energy (kcal/mol) at CCSD/cc-pVDZ theoretical level		Interaction energy (kcal/mol) at B3LYP/cc-pVTZ theoretical level	
	ZPE + BSSE corrected	BSSE corrected	ZPE + BSSE corrected	BSSE corrected
D1	-12.7	-14.64	-17.48	-19.21
D2	-7.44	-8.90	-8.64	-10.22
D3	-4.2	-5.31	-4.37	-5.41
D4	-3.31	-4.79	-4.23	-5.60
D5	-2.18	-3.59	-2.44	-3.81
T1	-19.74	-22.87	-25.10	-28.03
T2	-16.84	-19.92	-22.45	-25.38
T3	-16.29	-19.37	-22.3	-24.91
T4	-	-19.2	-21.47	-23.94
T5	-	-17.74	-19.81	-22.01
T6	-	-17.57	-19.44	-22.21
T7	-14.61	-17.48	-19.21	-21.78

Here, the absence of T4, T5, and T6 values at the CCSD/cc-pVDZ level is due to infrastructure limitations that prevented conducting frequency calculations specifically for those trimer structures.

As it is inferred from table 4.2, table 4.3 and table 4.6, when going from dimer D1 to trimer T1 the interaction energy of TGA clusters increases. The BSSE corrected and ZPE+BSSE corrected interaction energy/binding energy of D1 was found to be -14.64 kcal/mol, -12.7 kcal/mol and -19.21 kcal/mol, -17.48 kcal/mol at CCSD/cc-pVDZ and B3LYP/cc-pVTZ level of theory. Whereas, For T1 trimer the BSSE corrected and ZPE+BSSE corrected interaction energy was found to be -22.87, -19.74 and -

28.03kcal/mol, -25.10 kcal/mol at CCSD/cc-pVDZ and B3LYP/cc-pVTZ level of theory. While the computed average bond energy [IE/BE divided by number of H-bonds][47] (BSSE+ZPE corrected) for D1 dimer and T1 trimer was found to be -6.35 and -6.58 kcal/mol at CCSD/cc-pVDZ level and -8.74 and -8.36 kcal/mol at B3LYP/cc-pVTZ level of theory. The difference between the average bond energy and the dimer binding energy signifies the degree of hydrogen bond cooperativity.

4.3.2 LED Calculation

The calculation of the dominant contribution of interaction energy in dimers and trimers can be performed using LED (Localized Energy Decomposition) analysis.[32,33,48–50] This analysis allows for the determination of different contributing factors to the interaction energy in the modeled system. LED calculation has been carried out at DLPNO-CCSD(T)/cc-pVTZ level of theory. In line with the methodology employed by Jaworski and Hedin,[51] the interaction energy was dissected using the LED [48,49] procedure, as executed in ORCA.[52] This decomposition method, carried out within the DLPNO-CCSD(T) framework, facilitates a coherent and interpretable breakdown, and is as follows:

$$\Delta E = \Delta E^{HF} + \Delta E^{C} \quad (2)$$

$$= \Delta E^{HF} + \Delta E^{C\text{-}CCSD} + \Delta E^{C\text{-}(T)} \quad (3)$$

$$= \Delta E^{HF} + \Delta E^{C}_{disp} + \Delta E^{C}_{non-disp} + \Delta E^{C\text{-}(T)} \quad (4)$$

$$= \Delta E^{HF}_{ep-prep} + E_{elstat} + E_{exch} + \Delta E^{C}_{disp} + \Delta E^{C}_{non-disp} + \Delta E^{C\text{-}(T)} \quad (5)$$

As depicted by equation (2), the interaction energy is decomposed into two constituents: (ΔE^{HF}), stemming from the Hartree-Fock (HF) level of theory, and the correction (ΔE^{C}), which arises from electron correlation. The latter component is further divided into two parts: the interaction energy contribution ($\Delta E^{C\text{-}CCSD}$) calculated at the CCSD level, and ($\Delta E^{C\text{-}(T)}$) arising from perturbative triple excitations (T), as described by equation (3). The correlation interaction energy of CCSD is further broken down into two components: the London dispersion contribution (ΔE^{C}_{disp}) and the non-dispersive correlation contribution

($\Delta E^{C}_{non-disp}$), which encompasses factors like charge transfer, intra-fragment double excitations, and singles contributions (equation 4). The HF-interaction energy term is broken down into distinct components: the repulsive electronic preparation contribution ($\Delta E^{HF}_{ep-prep}$), along with the attractive electrostatic (E_{elstat}) and exchange (E_{exch}) contributions, as illustrated in equation 5. The simplified values of the interaction energies (IEs) in TGA dimers and trimers are presented in table 4.7. From table 4.7, it is evident that the electrostatic correlation energy is the most significant contributor across all TGA clusters, followed by the exchange correlation energy and the dispersion correlation energy.

Table 4.7: DLPNO-CCSD(T) based Local Energy Decomposition (LED) of energy terms for the TGA(GGC) Dimers and Trimers

System	ΔE_{int}	ΔE^{ref}_{int}	$\Delta E^{ref}_{el-prep}$	E_{elstat}	E_{exch}	ΔE^{C}_{int}	ΔE^{C-CCSD}_{disp}	$\Delta E^{C-CCSD}_{non-disp}$	$\Delta E^{C-(T)}_{int}$
D1	-23.4	-21.03	105.17	-110.35	-15.85	-2.37	-3.66	1.95	-0.66
D2	-15.9	-13.65	50.74	-55.88	-8.51	-2.25	-3.21	1.43	-0.47
D3	-11.6	-8.61	32.23	-34.92	-5.92	-2.99	-2.82	0.26	-0.43
D4	-14.82	-8.65	49.09	-48.42	-9.32	-6.17	-4.19	-1.01	-0.97
D5	-10.87	-6.58	28.7	-29.32	-5.96	-4.29	-3.45	-0.21	-0.63
T1	-37.76	-32.67	152.6	-161.53	-23.74	-5.09	-6.78	2.83	-1.14
T2	-35.81	-29.12	146.24	-152.34	-23.02	-6.69	-7.09	1.66	-1.26
T3	-35.4	-28.86	137.48	-144.35	-21.99	-6.54	-7.38	2.05	-1.21
T4	-35.18	-25.88	138.92	-141.66	-23.14	-9.3	-8.77	1.05	-1.58
T5	-33.14	-26.56	133.02	-138.07	-21.51	-6.58	-7.46	2.09	-1.21
T6	-35.18	-25.88	138.92	-141.66	-23.14	-9.3	-8.77	1.05	-1.58
T7	-31.58	-25.83	125.23	-131.03	-20.03	-5.75	-6.6	1.95	-1.1

All energies are in kcal/mol

4.3.3 Investigation of Intra/Inter-molecular H-bond Interactions in dimers of TGA

In order to gain insight into the different non-covalent intra/inter-molecular interactions, as well as sulfur-centered H-bonding present in TGA clusters, AIM (Atoms in Molecules) calculations were performed at the CCSD/cc-pVDZ level of theory. These

calculations involved the determination of electron density ($\rho(r)$) and Laplacian electron density ($\nabla^2\rho(r)$). According to Koch and Popelier, the bond critical points (BCP) provide information about the path of the H-bond (H-acceptor), with an electron density range between 0.002-0.040 a.u. and a Laplacian electron density range between 0.024-0.139 a.u. Topological analysis of the BCP revealed that no intramolecular H-bond was observed in the GGC and GAC conformers of TGA, possibly due to the interaction between the mercapto-H and carbonyl oxygen being quite weak and hence not captured in the AIM calculation. However, in the dimers and trimers of TGA, significant intermolecular H-bond interactions were observed, including sulfur-centered H-bonding. AIM calculations for the dimers indicated the presence of sulfur-centered intermolecular H-bonding, where sulfur acted as both a proton donor and acceptor. The strength of oxygen-centered H-bonding was particularly high in the D1 dimer, with a calculated energy of -8.86 kcal/mol, while in other TGA dimers, it ranged from -4 to -7 kcal/mol. The highest strength of sulfur-centered H-bonding was observed in the D2 and D5 dimers, around -3.0 kcal/mol, while in the D4 dimers, it was approximately -2.1 kcal/mol. Thus, it can be inferred that these intermolecular H-bond interactions contribute to the stability of the TGA dimers, with D1 being the most stable due to strong oxygen-centered H-bonding. The topological basin surfaces with Bond critical points (3, -1) of all TGA dimers are shown in figure 4.7.

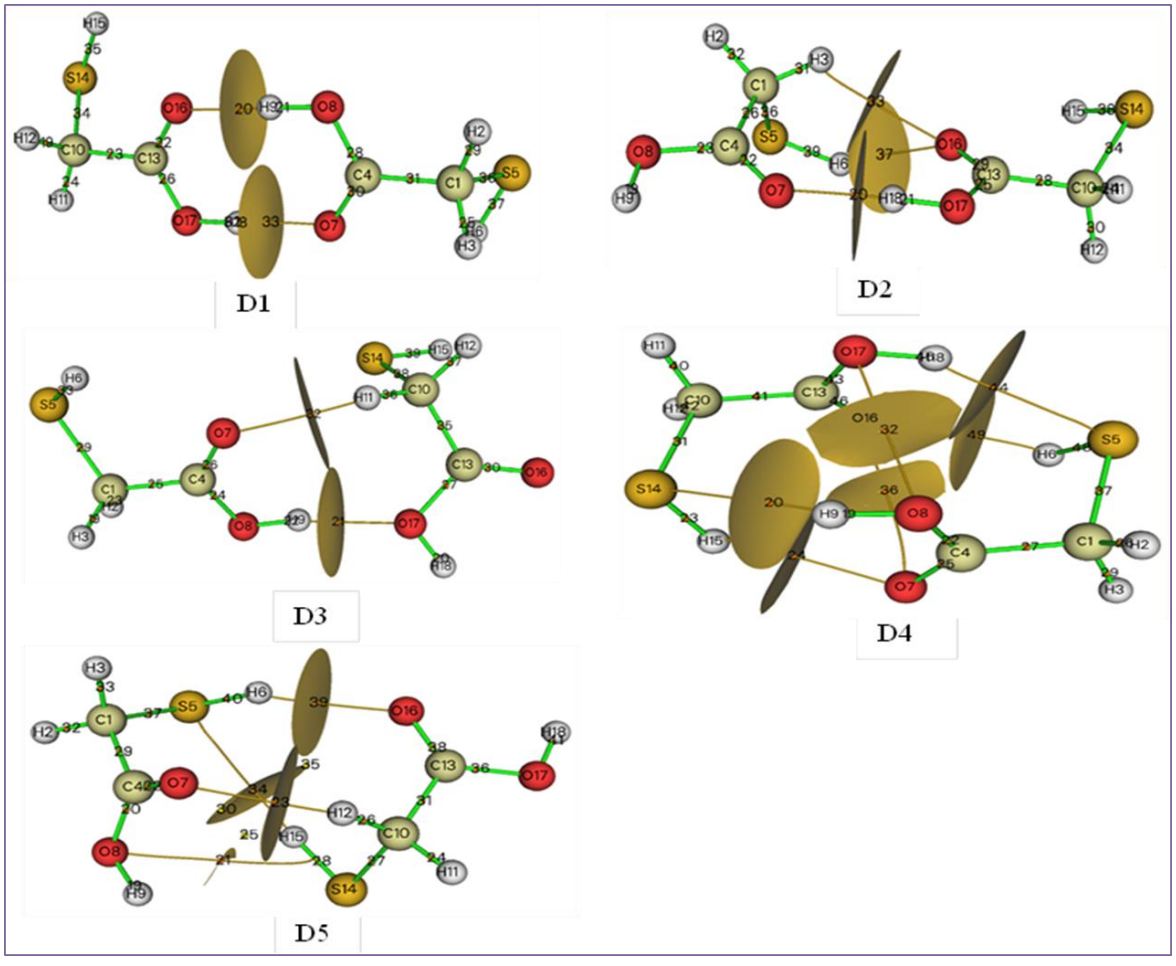

Figure 4.7: Topological basin surfaces with Bond critical points (3, -1) of TGA at CCSD/cc-pVDZ level for all the dimers(D1-D5) of TGA

The RDG analysis was also carried out for the visualization of non-covalent interactions observed in TGA clusters. To visually represent different interaction types, a color gradient was employed, where colors corresponded to specific ρ(r) and λ2 values and were filled in the RDG iso-surfaces depicted in Figure 4.8. The contour value was set at 0.5. These calculations and visualizations were performed using Multiwfn[53] and VMD[54] software. In Figure 4.8, blue regions indicate H-bond interactions, green regions represent van der Waals interactions, and red regions denote repulsive interactions. The RDG analysis yielded results consistent with the AIM calculations. In the D1 dimer, H-bonds formed between O-H—O and O—H-O moieties, along with weak H-bond

interactions between S-H—O. This is why the D1 dimer emerged as the most stable among all dimers. In the D2, D3, D4, and D5 dimers, weak intermolecular H-bond interactions were more prevalent compared to strong ones.

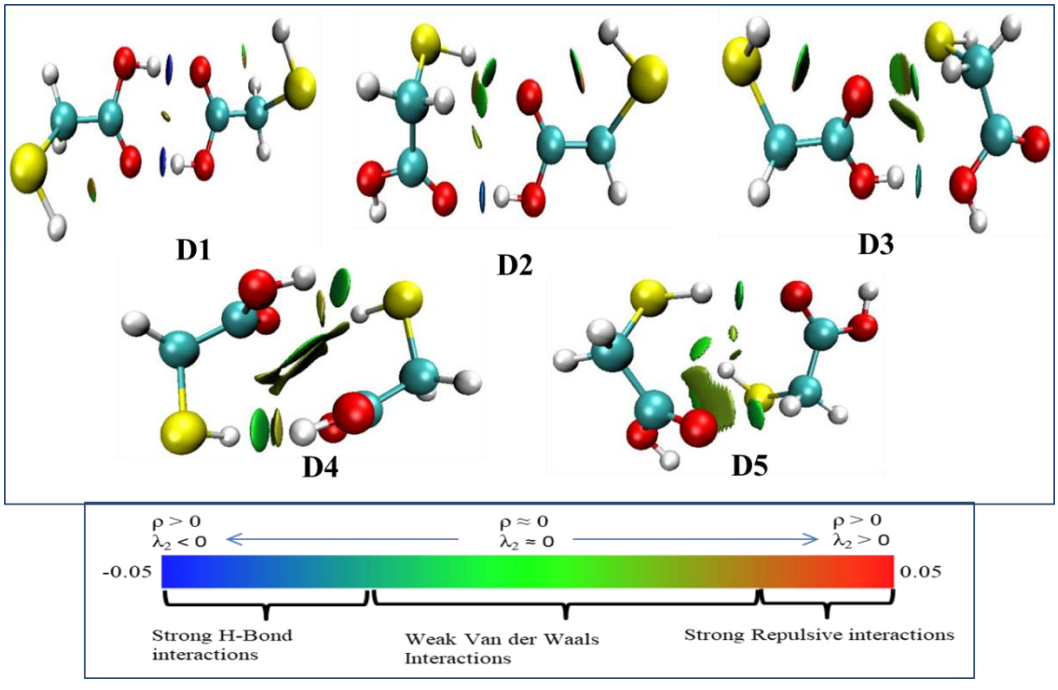

Figure 4.8: The visual diagram of RDG iso-surfaces for TGA dimers (D1-D5). Color gradient corresponds to the different types of interaction in respective clusters (dimers and trimers)

4.3.4 Investigation of Intra/Inter-molecular H-bond Interactions in trimers of TGA

Similar to dimers, in the AIM analysis of TGA trimers, non-covalent H-bond interactions of medium to weak strength were observed. Both oxygen and sulfur exhibited H-bond interactions in these trimers. Among all the trimer clusters, the T1 cluster of TGA was found to be the most stable, featuring three oxygen-centered H-bonds and one sulfur-centered H-bond. The strength of oxygen-centered H-bonds ranged from -8 to -12 kcal/mol, while the sulfur-centered H-bond was calculated to be -3.1 kcal/mol. In the other trimer clusters of TGA, both sulfur and oxygen-centered H-bonding were present. The range of oxygen-centered H-bonding varied between -6.5 to -9.5 kcal/mol, while the

range for sulfur-centered H-bonding was observed between -0.2 to -2.5 kcal/mol across all these trimer clusters. The topological basin surfaces with Bond critical points (3, -1) of all TGA trimers are shown in figure 4.9.

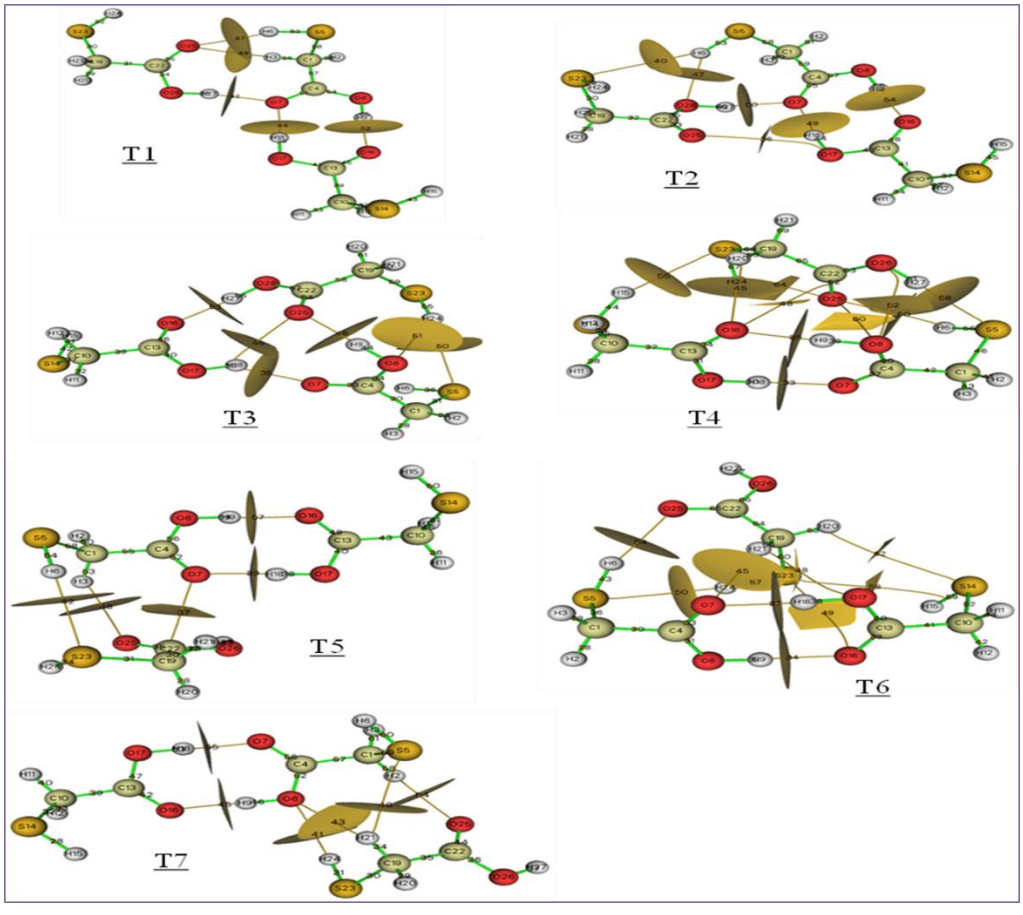

Figure 4.9: Topological basin surfaces with Bond critical points (3, -1) of TGA at CCSD/cc-pVDZ level for all the trimers (T1-T7) of TGA

The equation established by Emamian et al.[55] have been employed to estimate the energies of hydrogen bonds, given in the table 4.8. The approach by Espinosa and colleagues,[56] which estimates H-bond energies as E = V(r)/2, tends to overestimate H-bond energy and thus was not utilized. Based on the detailed AIM analysis of TGA dimers and trimers, it is inferred that although the strength of sulfur-centered H-bonding was comparatively weaker, yet contribute to the overall stability of TGA clusters in a significant manner. Also, on moving from dimers to trimers, while the strength of one

HB (H-bond) decreases, the strength of another HB increases. In the context of the T1 trimer, the introduction of a new TGA (HB) in D1 dimer to make T1 trimer leads to changes in the strength of the two existing HBs found in the D1 dimer. Based on this rationale, the presence of a cooperativity effect can be attributed, providing stability from monomers to dimers and further to trimer clusters. The calculated parameters of AIM analysis at BCP (3, -1) for all the TGA dimer and trimer clusters are summarized in table 4.8.

While doing RDG analysis, transitioning from dimers to trimers of TGA, the stability of the cluster increased with the presence of both strong H-bonds and weak H-bond/van der Waals interactions. Consequently, the T1 trimer was identified as the most stable among all trimers, featuring a relatively less strong S-centered HB (shown in green) coexists alongside 3 strong O-centered HBs (shown in blue), contributing significantly to the overall stability of the T1 trimer relative to the other trimer clusters. The RDG iso-surface corresponding to TGA trimer clusters are depicted in figure 4.10.

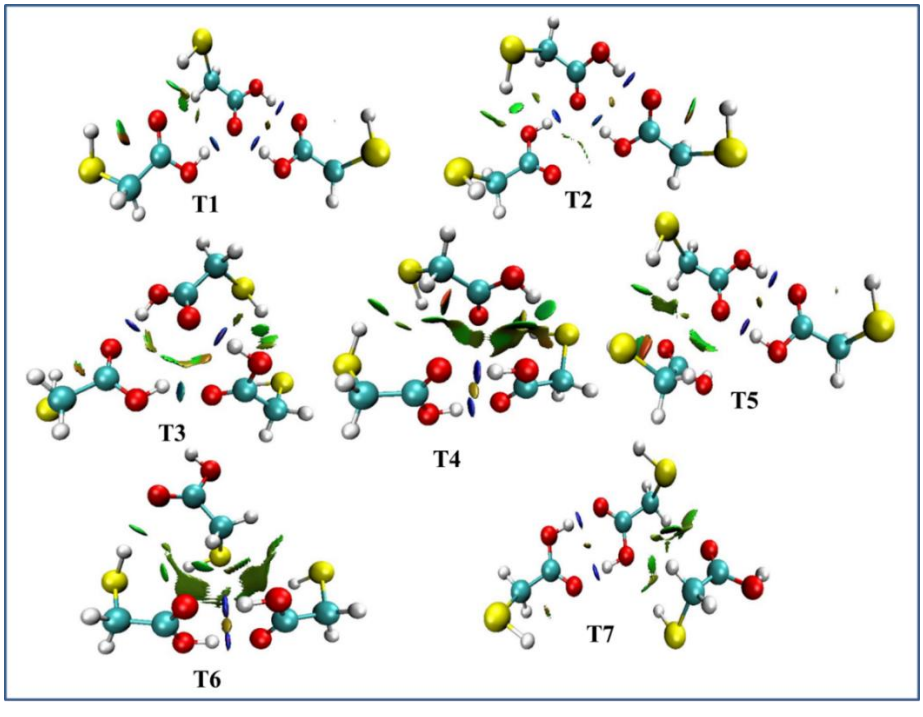

Figure 4.10: The visual diagram of RDG iso-surfaces for TGA trimers (T1-T7)

Table 4.8: Topological parameters for bonds of interacting atoms in TGA Dimers and Trimers: electron density (ρ_{BCP}), kinetic electron energy density (G_{BCP}), potential electron energy density (V_{BCP}), total electron energy density (H_{BCP}), Laplacian of electron density ($\nabla^2\rho_{BCP}$), estimated interaction energy (E_{int}) at bond critical point (BCP)

D1						
Critical Point number	**ρ_{BCP} [a.u.]**	**G_{BCP} [a.u.]**	**V_{BCP} [a.u.]**	**H_{BCP} [a.u.]**	**$\nabla^2\rho_{BCP}$ [a.u.]**	**E_{int} [kcal/mol]**
20[O16---H9-O8]	0.04307	0.03807	-0.03824	-0.00016	0.15165	-8.86
33[O7---H18-O17]	0.04307	0.03807	-0.03824	-0.00016	0.15164	-8.86
D2						
20[O7---H18-O17]	0.03379	0.03029	-0.02761	0.00268	0.13193	-6.79
33[O16---H3-C1]	0.00822	0.00681	-0.00603	0.00078	0.03042	-1.09
37[O16---H6-S5]	0.01254	0.00975	-0.00958	0.00016	0.03970	-2.05
D3						
21[O17---H9-O8]	0.02435	0.02107	-0.01838	0.00268	0.09506	-4.68
32[O7---H11-C10]	0.01245	0.00967	-0.00952	0.00014	0.03929	-2.03
D4						
20[S14---H9-O8]	0.01229	0.00697	-0.00650	0.00047	0.02978	-1.99
24[O7---H15-S14]	0.00862	0.00678	-0.00605	0.00073	0.03005	-1.18
32[O8---O17-C13]	0.00810	0.00728	-0.00668	0.00059	0.03153	-1.06
36[O16---O7-C4]	0.00430	0.00348	-0.00269	0.00078	0.01709	-0.21
44[S5---H18-O17]	0.01226	0.00696	-0.00649	0.00047	0.02972	-1.99
49[O16---H6-S5]	0.00865	0.00680	-0.00608	0.00072	0.03010	-1.18
D5						
21[O8---H15-S14]	0.00469	0.00368	-0.00273	0.00095	0.01856	-0.30
23[O7---H12-C10]	0.01266	0.00994	-0.00980	0.00014	0.04037	-2.08
34[S5---H15-S14]	0.00654	0.00358	-0.00321	0.00036	0.01581	-0.71
39[O16---H6-S5]	0.01292	0.00947	-0.00954	-0.00007	0.03759	-2.14
T1						
42[O7---H27-O26]	0.03321	0.02955	-0.02705	0.00250	0.12820	-6.66
44[O7---H17-O18]	0.03893	0.03417	-0.03313	0.00105	0.14089	-7.94
47[O26---H6-S5]	0.01304	0.01006	-0.00995	0.00011	0.04069	-2.16
49[O26---H3-C1]	0.00771	0.00636	-0.00556	0.00079	0.02862	-0.97
52[O16---H9-O8]	0.04482	0.03967	-0.04054	-0.00086	0.15525	-9.25
T2						
36[O25----O17]	0.00396	0.00413	-0.00303	0.00110	0.02096	-0.14
40[S23---H6-S5]	0.00451	0.00260	-0.00214	0.00047	0.01228	-0.26
47[O26---H6-S5]	0.00956	0.00711	-0.00694	0.00018	0.02917	-1.39
49[O7---H18-O17]	0.03357	0.02913	-0.02718	0.00194	0.12429	-6.74
50[O7---H27-O26]	0.03528	0.03103	-0.02937	0.00166	0.13078	-7.13
54[O16---H9-O8]	0.04522	0.04039	-0.04132	-0.00092	0.15790	-9.34
T3						
35[O7---H18-O17]	0.02506	0.02137	-0.01967	0.00170	0.09232	-4.84
45[O26---H18-O17]	0.00842	0.00765	-0.00692	0.00074	0.03359	-1.13

48[O25---H9-O8]	0.03976	0.03604	-0.03493	0.00111	0.14863	-8.13
50[S5---H24-S23]	0.00450	0.00267	-0.00211	0.00055	0.01288	-0.26
51[O8---H24-S23]	0.00849	0.00639	-0.00607	0.00032	0.02688	-1.15
53[O16---H27-O26]	0.04044	0.03727	-0.03593	0.00134	0.15448	-8.28
T4						
33[O7---H18-O17]	0.04186	0.03678	-0.03658	0.00020	0.14795	-8.59
38[O16---H9-O8]	0.04237	0.03705	-0.03718	-0.00013	0.14771	-8.71
45[O16---H24-S23]	0.00765	0.00633	-0.00563	0.00069	0.02811	-0.96
48[O16-----C22]	0.00462	0.00401	-0.00294	0.00106	0.02029	-0.28
50[O25-----O8]	0.00672	0.00592	-0.00516	0.00075	0.02670	-0.75
52[O8-----O26]	0.00945	0.00902	-0.00814	0.00088	0.03962	-1.36
55[S23---H15-S14]	0.00847	0.00469	-0.00434	0.00036	0.02024	-1.36
58[S5---H27-O26]	0.01365	0.00766	-0.00699	0.00067	0.03333	-2.30
60[O25---H6-S5]	0.00725	0.00584	-0.00483	0.00101	0.02742	-0.87
64[O25---H24-S23]	0.01443	0.01240	-0.01122	0.00117	0.05431	-2.47
T5						
39[O7---H18-O17]	0.04386	0.03891	-0.03936	-0.00045	0.15384	-9.04
42[S23---H6-S5]	0.00942	0.00517	-0.00486	0.00031	0.02192	-1.36
48[O25---H3-C1]	0.00810	0.00637	-0.00592	0.00045	0.02730	-1.06
57[O16---H9-O8]	0.04164	0.03669	-0.03638	0.00031	0.14799	-8.54
T6						
34[O16---H9-O8]	0.04185	0.03668	-0.03652	0.00015	0.14734	-8.59
37[O7---H18-O17]	0.04304	0.03805	-0.03826	-0.00020	0.15142	-8.86
45[O7---H21-C19]	0.01067	0.00833	-0.00816	0.00016	0.03395	-1.64
48[O17---H21-O19]	0.00520	0.00499	-0.00369	0.00129	0.02516	-0.41
49[S23----O16]	0.00372	0.00242	-0.00192	0.00050	0.01171	-0.08
50[S5---H24-S23]	0.00829	0.00452	-0.00419	0.00033	0.01939	-1.11
54[O25---H6-S5]	0.01278	0.00924	-0.00936	-0.00012	0.03648	-2.11
58[S23---H15-S14]	0.00437	0.00248	-0.00192	0.00056	0.01218	-0.23
62[S14---H20-C19]	0.00292	0.00184	-0.00136	0.00047	0.00924	-0.09
T7						
41[O8---H24-S23]	0.00806	0.00662	-0.00595	0.00067	0.02915	-1.05
43[O8---H21-C19]	0.00649	0.00553	-0.00472	0.00080	0.02533	-0.70
45[O16---H9-O8]	0.04427	0.03923	-0.03975	-0.00053	0.15481	-9.13
48[S5---H21-C19]	0.00499	0.00306	-0.00253	0.00053	0.01437	-0.37
54[O25---H2-C1]	0.01248	0.00971	-0.00959	0.00011	0.03926	-2.04
55[O7---H18-O17]	0.04275	0.03771	-0.03777	-0.00006	0.15057	-8.79

Here, numbers after atoms represent the label of respective atom (figure 4.5 and figure 4.6).

4.3.5 NBO analysis

The analysis of different electronic transitions, identification of the involved orbitals, and the assessment of intra/intermolecular interactions and charge transfer within a molecule and cluster can be performed using NBO calculations. NBO analysis revealed several noteworthy observations in the monomers, dimers and trimers of TGA. In both

the GGC and GAC monomers, there was a transfer of a lone pair of electrons from S5 to the π* orbital of the C4=O7 bond. Additionally, strong electron delocalization was observed in the carboxylic moiety, specifically involving non-bonding electrons (n) of O7, O8 atoms and sigma antibonding orbital (σ*), pi antibonding orbital (π*) of C4-O8, C4-O7 bonds i.e. nO7→σ*C4-O8 and nO8 → π*C4-O7 electron transfers respectively. Hyperconjugative interactions were also present in both monomers, albeit slightly stronger in the GGC conformer compared to the GAC conformer.

Moving on to the dimers, Dimer D1 exhibited intermolecular charge transfer between nO7→σ*H18-O17 and nO16→σ*H9-O8 antibonding orbitals, in addition to other intramolecular hyperconjugative interactions observed in individual monomers. In D2, a charge transfer was observed between nO7→σ*H18-O17 with a stabilization energy of 11.57 kcal/mol, along with another charge transfer between nO16→σ*(H6-S5) with a stabilization energy of 2.38 kcal/mol, where sulfur acted as a proton donor. In case of dimer D3, the charge transfer strength between nO7→σ*H6-S5 and nS14→σ*H9-O8 was very low, measured at 0.78 kcal/mol and 0.15 kcal/mol, respectively. Conversely, a strong intermolecular charge transfer was observed between nO17→σ*H9-O8, with a substantial E (2) stabilization energy of 10.75 kcal/mol. While in dimer D4, sulfur played the role of both proton donor and acceptor. Sulfur-centered charge transfer was observed between nS5→σ*H18-O17 and nS14→σ*H9-O8 (sulfur as proton acceptor) with stabilization energies ranging from 5 to 6 kcal/mol, as well as between nO7→σ*H15-S14 and nO16→σ*H6-S5 (sulfur as proton donor) with stabilization energies of 0.66-0.67 kcal/mol. This suggests that sulfur predominantly acts as a proton acceptor rather than a proton donor. However, in dimer D5, intermolecular charge transfer was observed between nS5→σ*H15-S14, where the sulfur of one TGA molecule donates its lone pair of electrons, while the sulfur atom of the second TGA molecule donates its proton. The strength of this interaction was calculated to be 2.08 kcal/mol, indicating a weak interaction. Another charge transfer involved oxygen donating its electron pair and sulfur donating its proton, specifically nO16→σ*H6-S5 with strength of 2.40 kcal/mol. This difference in charge transfer strength may explain the comparatively lower stability of

this dimer cluster among the others. Similar to the monomers, intramolecular hyperconjugative interactions were also observed in all of these dimer clusters.

In the case of trimer TGA clusters, both oxygen and sulfur atoms were participated in charge transfer among themselves, similar to the dimers of TGA. As expected, the strength of oxygen-centered charge transfer was higher than sulfur-centered charge transfer in the trimers as well. In the T1 trimer, strong interactions were formed between O16---H9-O8, O7---H27-O26, and O7---H18-O17, with E (2) stabilization energies ranging from 13 to 24 kcal/mol, indicating a very high interaction/charge transfer strength. Additionally, a weak charge transfer with a stabilization energy of 2.56 kcal/mol was observed between O25---H6-S5 in the T1 trimer cluster. On the other hand, in the T2 trimer, along with the O-centered charge transfer, a stronger S-centered charge transfer with a strength of 4.05 kcal/mol was observed compared to the T1 trimer. Similar patterns of strong O-centered and weak S-centered many charge transfer/donor-acceptor interactions were observed in other trimer clusters of TGA. These intermolecular charge transfer contribute to the stability of these trimer clusters. It is worth noting that as we move from dimers to trimers, not only does the number of intermolecular interactions increase, but also the strength of these interactions and the intramolecular hyperconjugative interactions, ensuring the stability of the TGA dimers to trimer clusters. The significant donor-acceptor interactions observed in the NBO analysis of monomers, dimers, and trimer clusters of TGA are provided in table 4.9a, 4.9b and 4.9c.

Table 4.9a: Some significant donor - acceptor NBO interactions in TGA monomers (GGC and GAC) with calculated second order stabilization energies E (2) kcal/mol at CCSD/cc-pVDZ level

Donor → Acceptor	**E(2) Kcal/mol**	
	GGC	**GAC**
σC1–H2 → π*C4–O7	4.88	-
σC1–H2 → σ*C4–O8	-	5.21
σC1–H3 → π*C4–O7	2.43	3.59
σC1–S5 → π*C4–O7	7.76	6.93
σS5–H6 → σ*C1–H2	2.48	2.43
σO8–H9 → σ*C1–C4	6.87	6.57

LP S5 → σ* C1–H3	4.57	4.37
LP S5 → σ*C1–C4	6.62	7.28
LP S5 → π*C4–O7	2.39	2.08
LP O7 → σ*C1–C4	27.68	27.99
LP O7 → σ*C4–O8	44.67	45.50
LP O8 → π*C4–O7	63.59	60.38

Here, LP = lone pair of electrons, σ = sigma bonding orbital, π = pi bonding orbital, π* = pi antibonding orbital and numbers after atoms represent the label of respective atom (figure 4.3).

Table 4.9b: Some significant donor - acceptor NBO interactions in TGA dimers (D1-D5) with calculated second order stabilization energies E (2) kcal/mol at CCSD/cc-pVDZ level

Donor → Acceptor	**E(2) kcal/mol**				
	D1	**D2**	**D3**	**D4**	**D5**
within unit 1					
σ C1-H2 → π*C4-O7	5.89	5.57	4.67	4.81	5.09
σ C1-H3 → π*C4-O7	4.83		8.34		
σ C1-H3 → σ*C4-O8	2.93	4.95		5.09	5.15
σ C1-C4 → σ*O8-H9	4.75	4.50	4.65	4.51	4.37
σ C1-S5 → π*C4-O7	6.31	8.89		7.70	8.39
σ C1-S5 → σ*C4-O8			3.64		
π C4-O7→ σ*C1-S5	1.51	2.01		2.61	2.37
σ C4-O8 → σ*C1-S5			1.96		
σ S5-H6 → σ*C1-H2	3.10		3.09	2.80	2.81
σ O8-H9 → σ*C1-C4	7.06	6.74	6.49		6.76
σ O8-H9 → σ*C4-O7		1.96	1.30	6.44	1.73
LP S5 → σ*C1-H3	4.46	2.13	6.72	5.20	4.53
LP S5 → σ*C1-C4	5.42	6.93	3.86	4.27	5.30
LP S5 → π*C4-O7	1.78	3.61		2.27	2.87
LP O7 → σ*C1-C4	22.72	16.97	23.93	23.82	23.05
LP O7 → σ*C4-O8	25.18	38.77	37.66	40.03	40.52
LP O7 → σ*S5-H6			0.78		
LP O8 → π*C4-O7	80.91	66.67	66.09	63.05	62.60
from unit 1 to unit 2					
LP O7 → σ*O17-H18	21.34	11.57			
LP O7 → σ*C10-H12					1.57
πC4-O7 → σ* S14-H15			0.18	0.11	
LP S5 → σ*O17-H18				5.99	
LP S5 → σ*S14-H15					2.08
LP O7 → σ* S14-H15			0.07	0.66	
from unit 2 to unit 1					
LP O16 → σ*O8-H9	21.34				
LP O16 → σ*S5-H6		2.38		0.67	2.40
LP O17 → σ* O8-H9			10.75		
LP S14 → σ*O8-H9			0.15	6.02	0.45

σ S14-H15 → π* C4-O7					0.15
within unit 2					
σ C10-H11 → π*C13-O16	5.89	5.05	5.22	4.80	5.96
σ C10-H11 → σ*S14-H15		1.69			
σ C10-H12 → π*C13-O16	4.83	8.79			3.20
σ C10-H12 → σ*C13-O17	2.93		5.90	5.09	3.93
σ C10-C13 → σ*O17-H18	4.75	4.80	4.02	4.51	4.39
σ C10-S14 → π*C13-O16	6.31		8.21		
σ C10-S14 → σ*C13-O17		3.44			
σ S14-H15 → σ*C10-H11	3.10	3.11	2.79	2.80	2.84
σ O17-H18 → σ*C10-C13	7.06	6.65	5.91	6.43	6.73
σ O17-H18 → π*C13-O16		1.23	1.70	1.34	1.81
LP S14 → σ*C10-H12	4.46	6.53	3.77	5.19	3.49
LP S14 → σ*C10-C13	5.42	4.04	6.10	4.28	5.62
LP S14 → π*C13-O16	1.78		2.94	2.27	2.37
LP O16 → σ*C10-C13	22.72	23.84	22.74	23.83	21.63
LP O16 → σ*C13-O17	25.18	35.62	45.42	40.03	41.04
LP O17 → π*C13-O16	80.91	72.75	51.68	63.05	63.07

Here, LP = lone pair of electrons, σ = sigma bonding orbital, π = pi bonding orbital, π* = pi antibonding orbital and numbers after atoms represent the label of respective atom (figure 4.5).

Table 4.9c: Some significant donor - acceptor NBO interactions in TGA trimers (T1-T7) with calculated second order stabilization energies E (2) kcal/mol at CCSD/cc-pVDZ level

Donor → Acceptor	**E(2) kcal/mol**						
	T1	**T2**	**T3**	**T4**	**T5**	**T6**	**T7**
within unit 1							
σ C1-H2 → π*C4-O7	5.61	6.05	5.13	3.99	5.32	5.27	5.82
σ C1-H3 → π*C4-O7	1.65	2.31			2.06		2.56
σ C1-H3 → σ*C4-O8	4.76	4.48	4.68	5.76	4.59	4.93	4.52
σ C1-C4 → σ*O8-H9	4.97	4.93	4.53	4.69	4.80	4.79	4.70
σ C1-S5 → π*C4-O7	9.33	8.69	7.94	6.58	8.36	8.39	8.51
π C4-O7 → σ*C1-C4	1.06	1.00			1.10		1.12
π C4-O7 → σ*C1-S5	1.71	1.89	2.27	2.47	1.76	2.10	2.04
σ C4-O8 → σ*C1-H3	1.07		1.12				

σ S5-H6 → σ*C1-S5		1.43					
σ O8-H9 → σ*C1-C4	6.88	7.23	6.55	6.73	6.92	6.99	6.66
σ O8-H9 → π*C4-O7	1.34	1.41		1.16			1.20
LP S5 → σ*C1-C4	6.87	6.71	5.43	4.18	6.60	5.75	5.32
LP S5 → π*C4-O7	3.81	3.17	2.86	1.57	3.42	2.95	2.88
LP O7 → σ*C1-C4	19.10	18.63	23.27	23.55	21.35	22.14	22.18
LP O7 → σ*C4-O8	28.18	30.18	34.11	26.34	24.45	23.94	25.86
LP O8 → π*C4-O7	87.58	85.72	70.41	73.62	82.32	81.82	76.02
from unit 1 to unit 2							
σ O8-H9 → π*C13-O16	0.40	0.42				0.35	0.38
LP O7 → σ*O17-H18	13.58	11.84	6.59	20.39	21.91	22.15	21.16
from unit 1 to unit 3							
LP S5 → π*C22-O25	0.09		0.52				
LP O7 → σ*O26-H27	12.93	11.28					
LP O7 → π*C22-O25					2.38		
LP O8 → σ*S23-H24			1.30				1.27
LP O8 → σ*O26-H27				0.51			
σ O8-H9 → π*C22-O25			0.33	0.12			
LP S5 → σ*S23-H24			0.52			3.01	
LP S5 → σ*O26-H27				7.98			
from unit 2 to unit 1							
π C13-O16 → σ*O8-H9	0.61						
σ O17-H18 → π*C4-O7	0.36	0.28	0.27				0.39
LP O16 → σ*O8-H9	23.25	22.96		21.66	20.00	20.42	22.83
within unit 2							
σ C10-H11 → π*C13-O16	5.86	5.10	5.71	4.52	5.81	5.05	5.91
σ C10-H12 → π*C13-O16	3.86	8.26	5.43		3.97		4.82
σ C10-H12 → σ *C13-O17	3.54		2.44	5.38		5.15	2.95
σ C10-C13 → σ*O17-H18	4.72	4.75	5.01	4.76	4.74	4.71	4.74
σ C10-S14 → σ *C13-O16	7.36		5.68	7.31	7.09	8.10	6.37
σ C10-S14 → σ*C13-O17	1.00	3.22	1.63				
π C13-O16 → σ *C10-S14	1.70		1.26	2.19	1.69	2.34	1.50
π C13-O16 → σ*C10-H12		1.09					
σ O17-H18 → σ *C10-C13	7.02	6.81	6.55	6.97	7.01	6.83	7.06
σ O17-H18 → π*C13-O16	1.26	1.17	1.05	1.25	1.19	1.13	1.21
LP S14 → σ*C10-H12	4.12	5.81	4.75	3.47	4.27	4.06	4.43
LP S14 → σ*C10-C13	5.62	5.03	5.23	6.69	5.48	5.75	5.44

LP S14 → π*C13-O16	2.37		1.62	2.65	2.23	2.70	1.79
LP O16 → σ*C10-C13	22.45	23.04	23.29	22.08	22.82	23.05	22.57
LP O16 → σ*C13-O17	24.83	24.41	28.02	23.87	25.79	25.84	24.61
LP O17 → π*C13-O16	79.83	78.51	79.87	82.40	80.69	76.74	80.06
from unit 3 to unit 1							
LP O25 → σ*S5-H6	2.56			0.40		2.24	
σ O26-H27 → π*C4-O7		0.29					
LP S23 → σ*S5-H6		0.84			4.05		
LP S23 → σ*O8-H9						0.14	
LP O26 → σ*S5-H6		1.55					
π C22-O25 → σ*O8-H9			2.93				
LP O25 → σ*O8-H9			12.26				
from unit 3 to unit 2							
LP O25 → σ*O17-H18		0.29	0.95				
σ O26-H27 → π*C13-O16			0.45				
LP S23 → σ*S14-H15				3.27		0.19	
from unit 2 to unit 3							
LP O16 → σ*O26-H27			14.78				
within unit 3							
σ C19-H20 → π*C22-O25	5.07	5.14	5.75	9.16	7.32	5.57	5.33
σ C19-C22 → σ*O26-H27	4.78	4.48	4.89	4.67	4.43	4.41	4.39
σ C19-S23 → σ*C22-O26	3.47			3.71	4.10		
σ C19-S23 → π*C22-O25		7.80				7.94	7.90
σ O26-H27 → σ*C19-C22	6.59	6.31	7.22	6.50	6.65	6.76	6.68
LP S23 → σ*C19-H21	6.47	4.18	3.22			3.08	2.41
LP S23 → σ*C19-H20				6.35	7.71		
LP S23 → σ*C19-C22	4.14	5.28	6.31	3.10	2.95	6.06	6.56
LP S23 → σ*C22-O26	0.54						
LP S23 → π*C22-O25		2.78	3.05			2.82	3.17
LP O25 → σ*O26-H27	0.52	0.60	0.74				
LP O25 → σ*C19-C22	23.90	23.81	6.18	23.79	24.36	21.31	22.00
LP O25 → σ*C22-O26	35.87	39.93	33.78	38.14	40.89	40.84	40.91
LP O25 → σ*S23-H24	0.72			1.29			
LP O26 → π*C22-O25	71.38	63.22	81.67	66.24	61.10	63.11	62.66

Here, LP = lone pair of electrons, σ = sigma bonding orbital, π = pi bonding orbital, π* = pi antibonding orbital and numbers after atoms represent the label of respective atom (figure 4.6).

4.3.6 Charge analysis

In order to assess the influence of intramolecular charge transfer on the atomic charges within TGA clusters, ESP[MK](Merz kollman) charge calculations[57] were conducted at the CCSD/cc-pVDZ level of theory. It was observed that in the case of GGC, the S5 atom exhibited a slightly more negative charge compared to the GAC conformer, while H16 displayed a higher positive charge, indicating an interaction between the S-H---O moieties. In all dimer systems, with the exception of D2, the O7 atom exhibited a comparatively lower negative charge than O8. This discrepancy in D2 arises from the fact that O8 does not engage in interactions with other molecules, leading to its relatively higher negative charge. Whereas the lower negative charge could be attributed to the involvement of O7 and O16's lone pairs of electrons in H-bond formation. Consequently, H9 and H18 exhibited higher positive charges compared to other H atoms that were not attached to oxygen atoms. On the other hand, H6 and H15 displayed lower positive charges as these H atoms were influenced by both the lone pairs of electrons from sulfur and oxygen.

This observation indicates S-centered H-bonding between the S-H—O moieties. Similarly, in the T1 trimer cluster, the O25 atom had a lower negative charge due to the attraction of its lone pair of electrons by the adjacent H atom of the S-H bond. A similar trend was observed for the O16 atom, which exhibited a lower negative charge than the O17 atom. In the case of sulfur atoms, S5 and S14 had lower negative charges compared to S23, possibly due to O---H-S interactions involving S5 and S14 atoms. In the case of the S23-H24---O25 interaction, the lone pair of O25 may interact with both H6 and H24 atoms due to their close proximity, resulting in a higher negative charge on S23. This explains why H27, H9, and H18 displayed higher positive charges compared to other H atoms. Similarly, the charges on sulfur and oxygen atoms in the other six trimer cluster systems (T2, T3, T4, T5, T6, and T7) indicated the presence of S-centered H-bonds in addition to O-centered H-bonds. The charge values for each atom in all TGA systems, including monomers, dimers, and trimers are provided in the table 4.10a, 4.10b and 4.10c and their visual representation (individual and relative), are shown in figure 4.11. These results strongly support the findings from AIM, NCI, and NBO analyses.

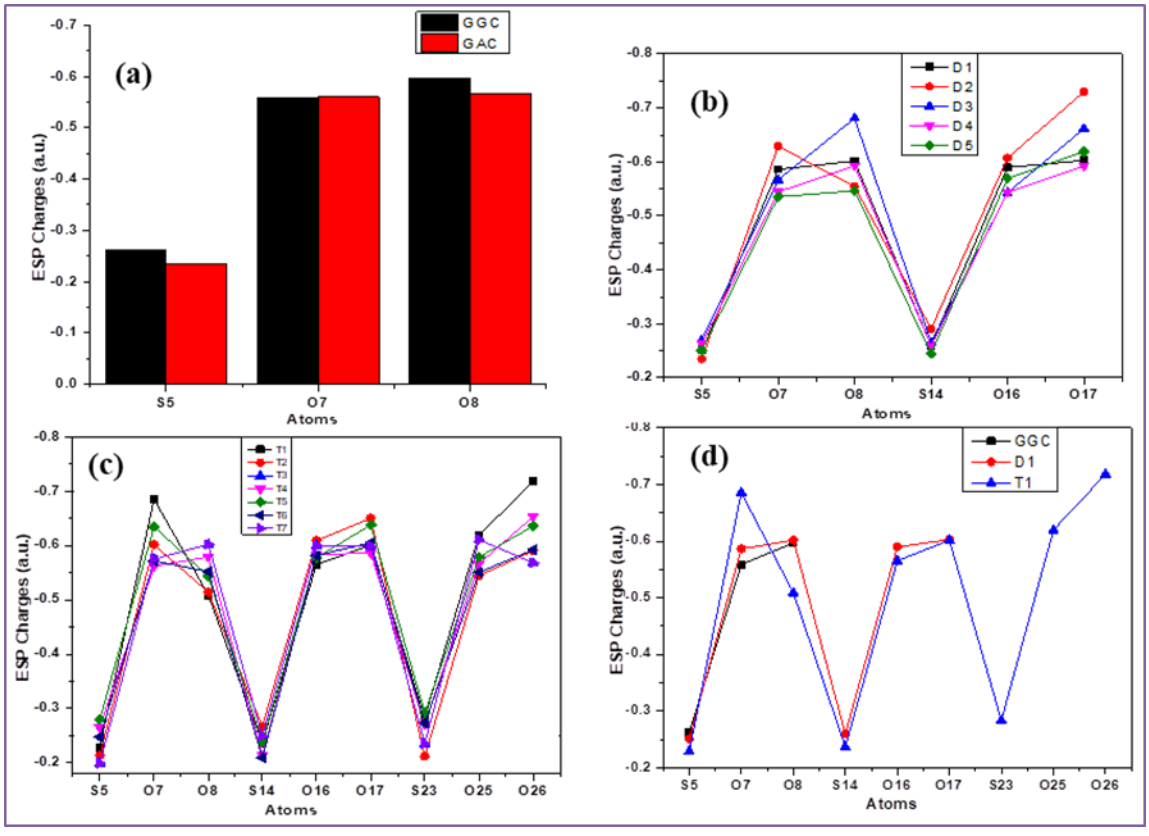

Figure 4.11: Charge distribution plot of ESP[MK] charges for TGA monomers (GGC and GAC) [a], dimers (D1-D5) [b] and trimers(T1-T7) [c] and comparison among GGC, D1 and T1[d]; the number after atoms represent the label of that atom

Table 4.10a: The ESP[MK] charge values [a.u.] on each atom of both the conformers (GGC & GAC) of TGA at CCSD/cc-pVDZ level of theory

Atoms	ESP[MK] Charge values(a.u.)	
	GGC	GAC
C1	-0.223	-0.322
H2	0.209	0.218
H3	0.103	0.149
C4	0.693	0.705
S5	-0.262	-0.234
H6	0.202	0.189
O7	-0.558	-0.559
O8	-0.596	-0.565
H9	0.433	0.420

Here, number after atoms represents label of that atom (figure 4.3).

Table 4.10b: The ESP[MK] charge values [a.u.] on each atom of all dimers (D1-D5) clusters of TGA at CCSD/cc-pVDZ level of theory

Atom	ESP[MK] charge values (a.u.) on dimers cluster of TGA				
	D1	D2	D3	D4	D5
C1	-0.304	-0.387	-0.345	-0.219	-0.313
H2	0.219	0.233	0.228	0.190	0.213
H3	0.130	0.144	0.138	0.095	0.123
C4	0.734	0.753	0.842	0.715	0.711
S5	-0.250	-0.235	-0.270	-0.263	-0.250
H6	0.204	0.221	0.205	0.220	0.234
O7	-0.586	-0.628	-0.566	-0.544	-0.535
O8	-0.601	-0.554	-0.680	-0.592	-0.546
H9	0.454	0.430	0.468	0.398	0.381
C10	-0.257	-0.319	-0.370	-0.247	-0.246
H11	0.204	0.228	0.233	0.198	0.202
H12	0.116	0.135	0.160	0.104	0.108
C13	0.730	0.839	0.751	0.721	0.746
S14	-0.259	-0.290	-0.265	-0.259	-0.244
H15	0.204	0.210	0.215	0.220	0.166
O16	-0.589	-0.607	-0.542	-0.544	-0.569
O17	-0.602	-0.729	-0.661	-0.592	-0.619
H18	0.452	0.554	0.460	0.398	0.439

Here, number after atoms represents label of that atom (figure 4.5).

Table 4.10c: The ESP[MK] charge values [a.u.] on each atom of all trimers (T1-T7) clusters of TGA at CCSD/cc-pVDZ level of theory

Atoms	ESP[MK] Charge values (a.u.) on trimers cluster of TGA						
	T1	T2	T3	T4	T5	T6	T7
C1	-0.428	-0.408	-0.373	-0.243	-0.233	-0.280	-0.373
H2	0.233	0.237	0.222	0.199	0.192	0.196	0.222
H3	0.163	0.165	0.139	0.109	0.091	0.117	0.139
C4	0.767	0.729	0.784	0.703	0.728	0.724	0.784
S5	-0.228	-0.213	-0.199	-0.265	-0.280	-0.247	-0.199
H6	0.227	0.173	0.187	0.227	0.223	0.217	0.187
O7	-0.685	-0.601	-0.575	-0.562	-0.634	-0.572	-0.575
O8	-0.508	-0.514	-0.602	-0.579	-0.543	-0.55	-0.602
H9	0.398	0.409	0.443	0.419	0.398	0.408	0.443
C10	-0.347	-0.361	-0.340	-0.381	-0.356	-0.435	-0.340
H11	0.233	0.243	0.223	0.237	0.236	0.253	0.223
H12	0.141	0.143	0.131	0.133	0.134	0.151	0.131
C13	0.737	0.837	0.801	0.762	0.791	0.791	0.801
S14	-0.236	-0.266	-0.249	-0.213	-0.238	-0.209	-0.249
H15	0.204	0.211	0.204	0.171	0.200	0.213	0.204
O16	-0.565	-0.609	-0.600	-0.583	-0.578	-0.582	-0.600

O17	-0.601	-0.650	-0.599	-0.586	-0.638	-0.605	-0.599
H18	0.476	0.473	0.434	0.452	0.465	0.427	0.434
C19	-0.349	-0.357	-0.373	-0.255	-0.239	-0.074	-0.373
H20	0.229	0.219	0.232	0.158	0.111	0.137	0.232
H21	0.145	0.130	0.145	0.191	0.226	0.070	0.145
C22	0.858	0.749	0.760	0.723	0.799	0.654	0.760
S23	-0.283	-0.211	-0.235	-0.271	-0.292	-0.272	-0.235
H24	0.215	0.192	0.179	0.206	0.209	0.176	0.179
O25	-0.619	-0.544	-0.611	-0.566	-0.578	-0.550	-0.611
O26	-0.718	-0.590	-0.568	-0.653	-0.635	-0.592	-0.568
H27	0.538	0.414	0.437	0.465	0.441	0.434	0.437

Here, number after atom represents label of that atom (figure 4.6).

Moreover, to visualize the distribution of positive and negative electrostatic potentials in TGA, ESP mapping was performed on the optimized structures of all TGA monomers, dimers, and trimers clusters as depicted in figure 4.12. The ESP mapping was conducted at the CCSD/cc-pVDZ level of theory. In the color scale, red indicates regions of minimum electrostatic potential, making them susceptible to electrophilic attacks, while the blue end represents regions of maximum electrostatic potential, indicating vulnerability to nucleophilic attacks. Analysis of the ESP maps for TGA monomers revealed that negative potential regions were located on the carbonyl group of the molecule, whereas positive electrostatic potential regions were found over the OH moiety. In the case of the most stable dimer, D1 cluster, the negative potential regions were predominantly present on the oxygen atoms, while positive electrostatic potential regions were observed on the S-H and C-H moieties of D1. Similarly, in the most stable trimer, T1, more negative potential regions were located on the oxygen atoms, with relatively less negative potential observed on the sulfur atoms. The positive electrostatic potential regions were again situated on the S-H and C-H moieties of the T1 cluster.

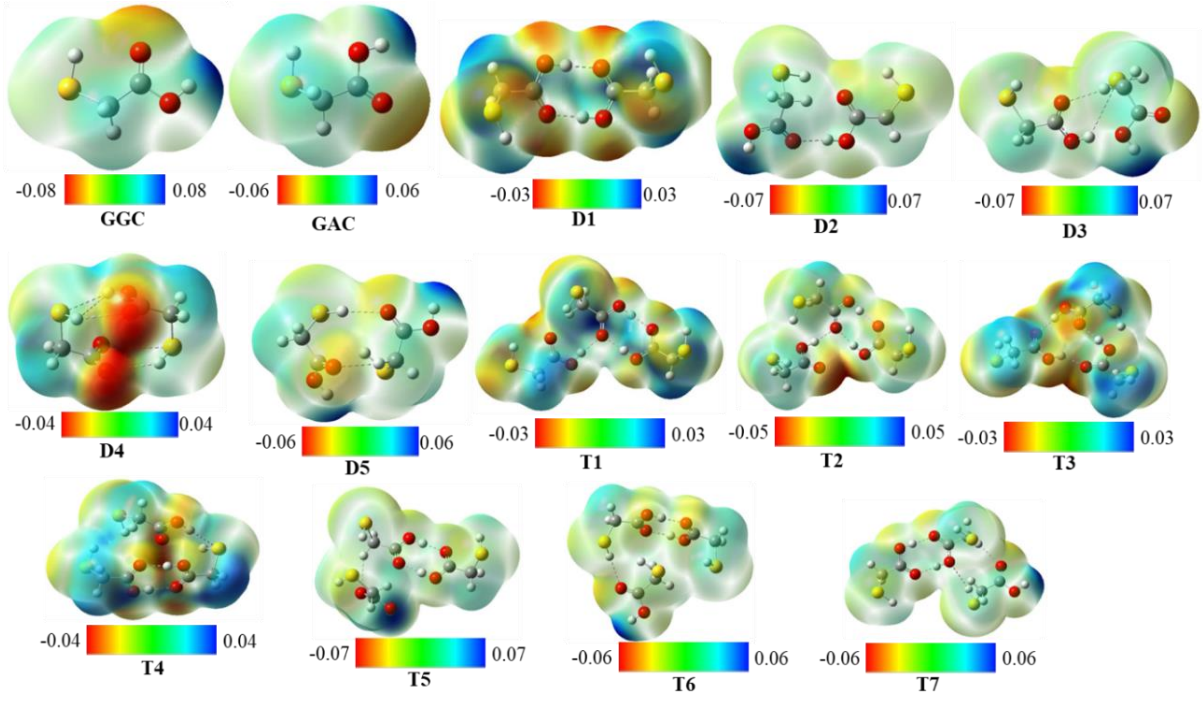

Figure 4.12: ESP map on optimized geometries of TGA monomers, dimers and trimers at CCSD/cc-pVDZ level of theory

4.3.7 FMO analysis

The HOMO-LUMO (H-L) gap is a well-known parameter used to assess the kinetic stability and chemical reactivity of molecules.[58] A smaller H-L gap indicates higher reactivity, while a larger gap signifies lower reactivity. In this study, the ground state properties of TGA were utilized to calculate the H-L gap. FMO (frontier molecular orbital) calculations were performed for all TGA monomers, dimers, and trimers clusters at the CCSD/cc-pVDZ level of theory. In FMO analysis, the FMO energy parameters of TGA monomers showed insignificant differences. This can be attributed to the minimal energy difference between the two monomers, which is only 0.16 kcal/mol. However, GGC conformer exhibited slightly lower chemical hardness and electronegativity compared to GAC, indicating increased reactivity in GGC. Whereas, the HOMO-LUMO gap slightly decreased from monomers to dimers to trimers, signifying an increased system reactivity. Though kinetic stability decreases from monomer to dimer to trimer, there is a simultaneous elevation in thermodynamic stability. As chemical hardness

characterizes a chemical species' resistance to electron cloud polarization or deformation—a pivotal gauge of stability and reactivity. In other words, chemical hardness serves as an indicator of the stability of the resulting complex or system. The elevation in hardness from monomers to both dimers and trimers underpins the stability of the formed cluster. Moreover, the electrophilicity index decreased from monomers to dimers to trimers, providing further evidence for the stability of dimer and trimer cluster systems. The computed FMO energy parameters and iso-surfaces of FMO orbitals for all TGA monomers, dimers and trimers clusters are shown in table 4.11 and figure 4.13.

Table 4.11: Computed energy (eV) parameters of TGA monomers, dimers and trimers at CCSD/cc-PVDZ level of theory

Systems	**Energy Parameters**							
	E_{HOMO} (IP) [eV]	E_{LUMO} (EA) [eV]	HOMO-LUMO gap [eV]	Dipole moment (D)	Hardness (η) [eV]	Chemical potential(μ) [eV]	Electron egativity (χ) [eV]	Electrophilicity index(ω) [eV]
GGC	-9.96	4.21	14.17	2.09	-2.875	-7.085	-2.88	-8.73
GAC	-10.14	3.89	14.03	2.18	-3.125	-7.015	-3.13	-7.87
D1	-10.15	3.69	13.84	1.95	-3.23	-6.92	-3.23	-7.42
D2	-9.86	3.61	13.47	2.22	-3.13	-6.74	-3.13	-7.26
D3	-9.87	3.69	13.56	2.14	-3.09	-6.78	-3.09	-7.45
D4	-10.28	3.63	13.91	1.07	-3.32	-6.96	-3.32	-7.28
D5	-10.05	3.66	13.71	0.95	-3.19	-6.86	-3.19	-7.35
T1	-9.92	3.49	13.41	2.65	-3.21	-6.70	-3.21	-6.99
T2	-10.02	3.46	13.48	2.63	-3.28	-6.74	-3.28	-6.92
T3	-10.06	3.56	13.62	2.16	-3.25	-6.81	-3.25	-7.18
T4	-9.94	3.58	13.52	2.77	-3.18	-6.76	-3.18	-7.18
T5	-9.92	3.66	13.58	3.45	-3.13	-6.79	-3.13	-7.36
T6	-10.00	3.52	13.52	1.55	-3.24	-6.76	-3.24	-7.05
T7	-9.95	3.65	13.60	0.82	-3.15	-6.80	-3.15	-7.35

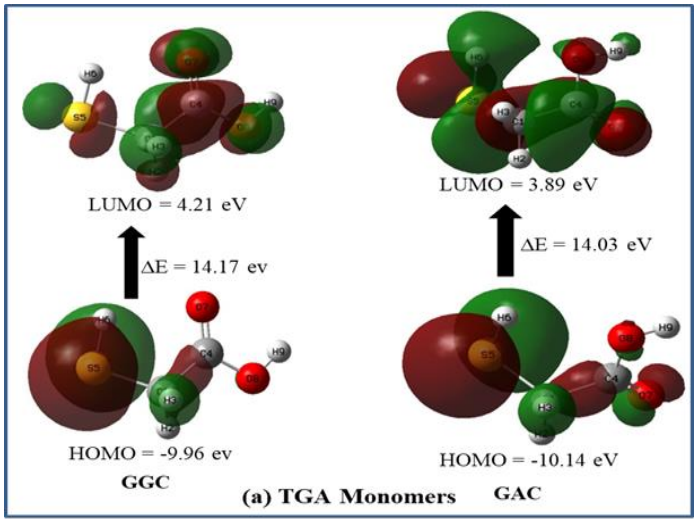
LUMO = 4.21 eV
ΔE = 14.17 ev
HOMO = -9.96 ev
GGC
LUMO = 3.89 eV
ΔE = 14.03 eV
HOMO = -10.14 eV
GAC
(a) TGA Monomers

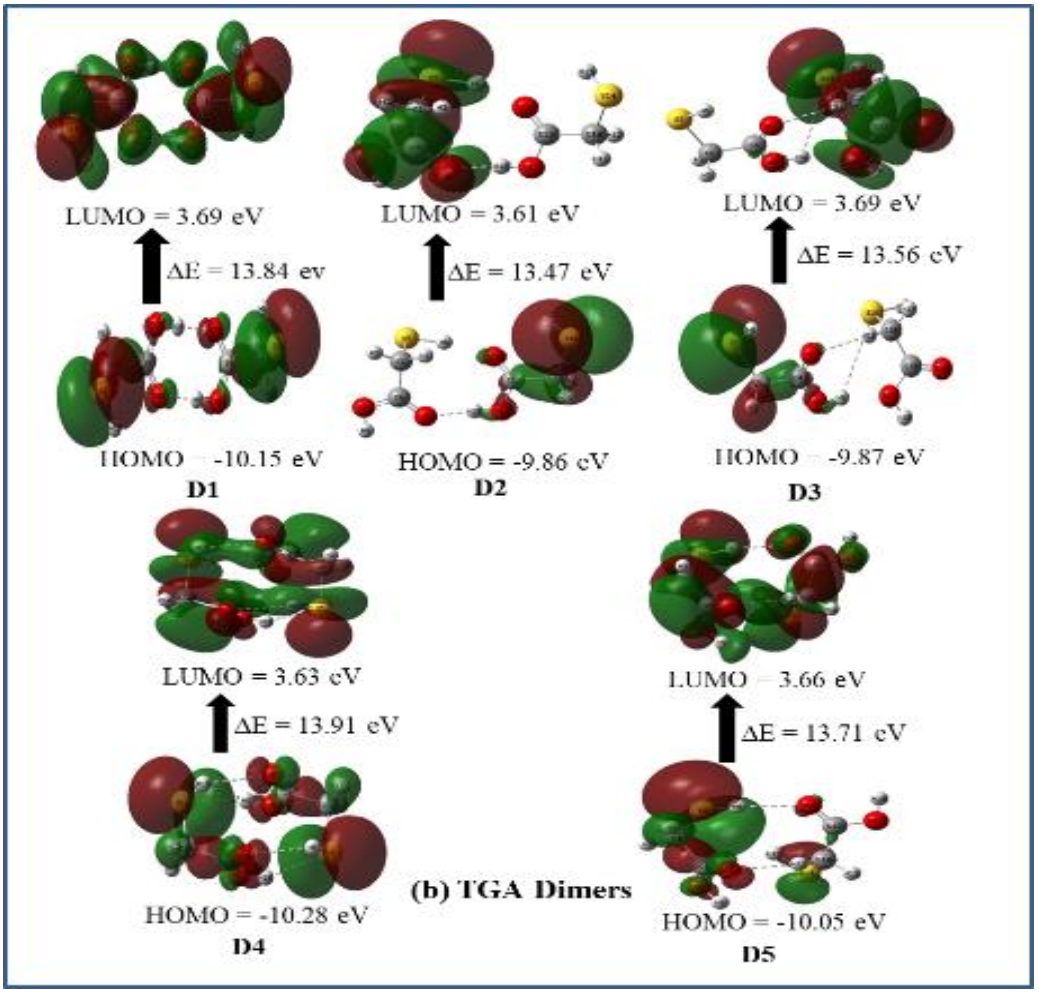
LUMO = 3.69 eV
ΔE = 13.84 ev
HOMO = -10.15 eV
D1
LUMO = 3.61 eV
ΔE = 13.47 eV
HOMO = -9.86 eV
D2
LUMO = 3.69 eV
ΔE = 13.56 eV
HOMO = -9.87 eV
D3
LUMO = 3.63 eV
ΔE = 13.91 eV
HOMO = -10.28 eV
D4
LUMO = 3.66 eV
ΔE = 13.71 eV
HOMO = -10.05 eV
D5
(b) TGA Dimers

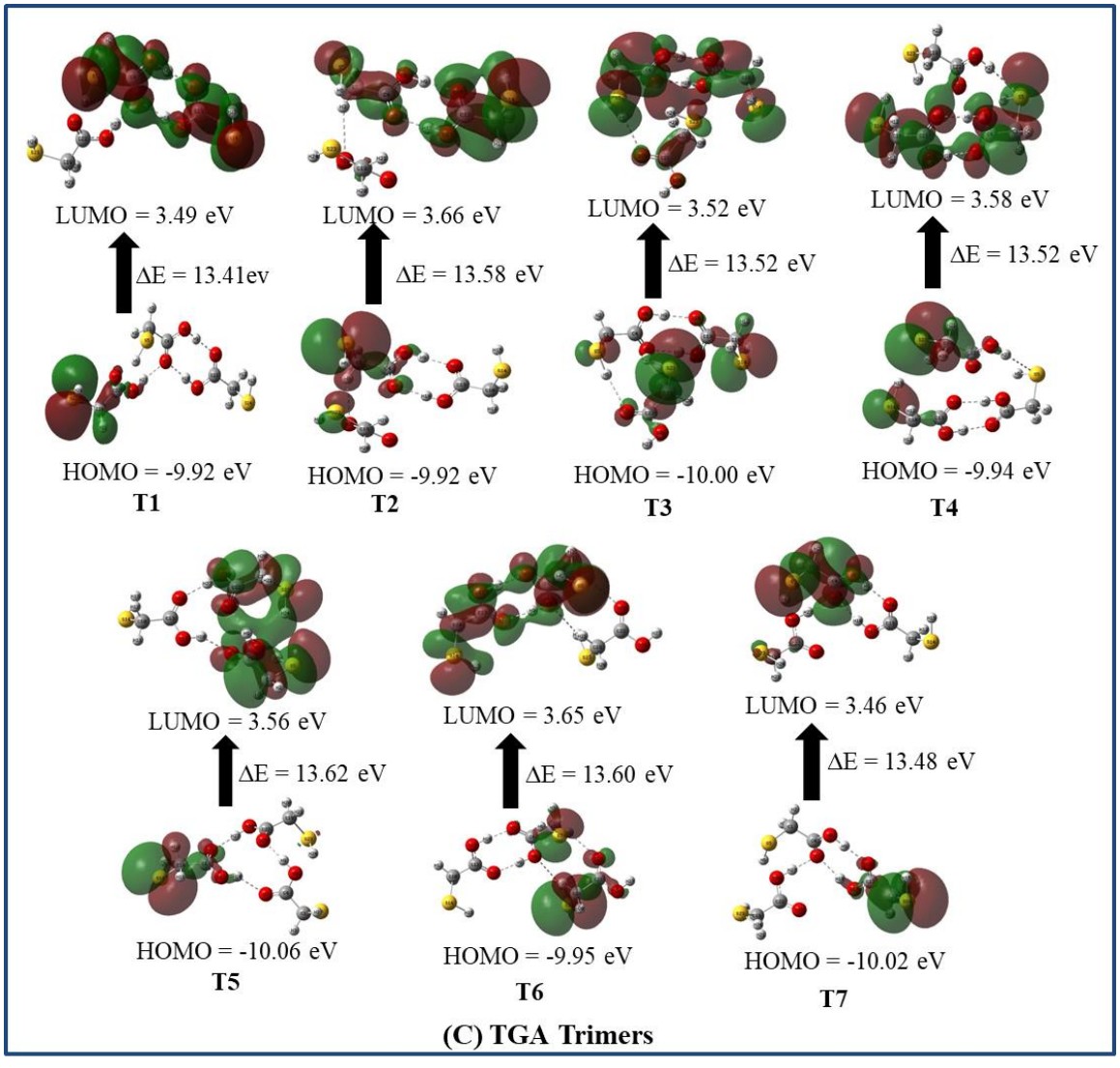

Figure 4.13: FMO iso-surface of TGA (a) monomers (GAC), (b) dimers (D2-D5) and (c) trimers (T2-T7) at CCSD/cc-pVDZ level of theory

4.3.8 Normal mode analysis

Non-covalent interactions typically cause a shift in the frequencies of one molecule when it interacts with another molecule within a cluster.[59] Vibrational frequency shifting is more pronounced in the presence of hydrogen bonding, whereas van der Waals interactions result in smaller frequency shifts. The S-H frequency of the most stable monomer, GGC, was observed at 2673 cm^{-1}, which closely matches the experimentally reported S-H vibrational mode range (2565-2570 cm^{-1}).[16] The O-H and C=O vibrational

modes were observed at 3731 and 1821 cm^{-1}, respectively. In the case of the most stable dimer of TGA, named D1, a significant change in the O-H frequency was observed due to the formation of a strong hydrogen bond between the carboxylic moieties of the two monomers. The dimer D1 exhibited a red shift of 608 cm^{-1} in the O-H frequency compared to its monomer. However, the SH peak in D1 showed little difference compared to the monomer. In the D2 dimer, the presence of a red shift in one of the S-H and O-H frequencies confirms the existence of both S-H---O and O---H-O hydrogen bonds. Similarly, in the D3 dimer, red shifts were observed in both O-H and S-H vibrational modes of both TGA monomers, providing further evidence for the presence of O-H---S and S-H---O hydrogen bonds.

Likewise, in the D4 and D5 dimers, the red shift in the S-H mode confirms the presence of S-centered hydrogen bonding. In addition to TGA dimers, TGA trimers also exhibited red shifts in S-H and O-H vibrational modes, indicating the presence of both oxygen-centered and sulfur-centered hydrogen bonds within the trimers. These hydrogen bonds play a crucial role in stabilizing the TGA clusters. It is to be noted that while moving from dimer to trimer as D1 to T1, the strength of OH stretching vibrational mode changes as the red shift was observed in one OH mode while the blue shift in the other OH stretching mode with the introduction of new H-bond in the trimer T1. This also suggest that cooperativity exists in the TGA clusters. One way to conveniently quantify the cooperative behavior of harmonic frequencies is by using the following expression[60] :

$$\text{Cooperativity} = \Delta\nu = [(\nu) - \nu(\text{monomer})] \qquad (6)$$

Here, $\Delta\nu$ represents the extent of frequency deviation within the cluster compared to the monomer. For each cluster, the average frequency shift $\Delta\nu$ is calculated as the difference between the average stretching frequency of the O–H bond in the cluster (ν) and the frequency of the individual monomers. The OH vibrational frequency decreases both in dimers and trimers clusters of TGA to that of monomer (GGC). Though the average shift in OH frequency in case of D1 dimer and T1 trimer clusters was obtained to be 608 cm^{-1} and 524.7 cm^{-1}. Also, from monomer to dimer to trimer the SH frequency decreases

though the shift is not so strong like the OH frequency. The average shift in SH frequency in case of D1 dimer and T1 trimer clusters was obtained to be 2 cm^{-1} and 12.3 cm^{-1}, respectively. These finding too suggests the existence of cooperativity as well as S-centered H-bonding among TGA clusters. The frequency calculations for TGA monomers, dimers and trimers were conducted using the B3LYP/cc-pVTZ//CCSD/cc-pVDZ level of theory. The comparison in SH, OH and C=O vibrational modes in monomer, dimers and trimers are presented in table 4.12 while all vibrational modes with their assignment are given in the table 4.13a, 4.13b and 4.13c.

Table 4.12: Calculated and experimental selective IR vibrational modes of TGA monomer (GGC), dimers (D1-D5) and trimers (T1-T7) at B3LYP/cc-pVTZ//CCSD/cc-pVDZ level of theory

Systems	Calculated Vibrational modes (cm^{-1})		
	ν_{S-H}	ν_{O-H}	$\nu_{C=O}$
GGC	2673.7	3731.4	1821.4
D1	2671.8	3123	1755.3
D2	2651.3	3355.2	1783.1
	2670.8	3733.4	-
D3	2666.3	3555	1792
	2675.4	3736.7	1830.8
D4	2665.1	3568.5	1809.5
D5	2609.7	3734.4	1789.8
	2651.2	3736.2	1802.3
T1	2643.1	3012.7	1669.4
	2671	3211.4	1742
	-	3396	1775.2
T2	2660.5	2970.3	1675
	2668.8	3251.3	1742.3
	2672.1	3415.5	1803.4
T3	2667.4	3192.6	1748
	2670.2	3252.5	1765.6
	2672	3365.3	-
T4	2616.8	2992.6	1756.1
	2652.2	3511	1791
	2667	-	-
T5	2611.2	3011.1	1749.8
	2671.4	3136.2	1810.6
	2675.4	3744.3	-

T6	2610.5	3021.4	1750.6
	2644.5	3735.3	1790.3
	2671.3	3132.8	-
T7	2664.1	2995.8	1753.2
	2667	3111.7	1799.5
	2671.1	3737.6	-
Experimental vibrational modes (cm^{-1})[16]	**2565**	**3350**	**1676**

Note: ν=stretching vibrational mode

Table 4.13a: Calculated IR vibrational modes of TGA monomers (GGC & GAC) at B3LYP/cc-pVTZ//CCSD/cc-pVDZ level of theory

GGC	GAC	Assignment[#]
732.6	679.4	$\nu_{CS} + \delta_{SH} + \delta_{OH}$
884.3	883.2	$\nu_{CC} + \delta_{OH}$
1141.2	1140.7	$\nu_{CO} + \tau_{CH2} + \delta_{OH}$
1459.7	1463.0	δs_{CH2}
1821.4	1824.3	$\nu_{C=O + OH\ bend}$
2673.7	2676.5	ν_{SH}
3052.2	3084.7	ν_{sCH2}
3127.3	3153	ν_{asCH2}
3731.4	3744	ν_{OH}

[#]: ν = stretching, νs = symmetric stretching, νas = asymmetric stretching, δs = scissoring and δ = bending, τ = twisting vibrational modes

Table 4.13b: Calculated IR vibrational modes (cm^{-1}) of TGA dimers (D1-D5) at B3LYP/cc-pVTZ//CCSD/cc-pVDZ level of theory

D1	D2	D3	D4	D5	Assignment[#]
694.7	674.4	670	709.7	685.4	$\nu_{CS} + \delta_{OCO}$
	690.7	737.3		687.4	
922.6	896.7	863.1	886.4	887.4	ν_{CC}
	905.6	896.5		888.7	
1348	1297.4	1126.3	1387	1146.6	$\nu_{CO} + \delta_{OH} + \delta_{COH}$
	1388.4	1176.9	1389	1152.4	
1484.6	1465.5	1461	1466.5	1466.7	$\delta s_{CH2} + \delta_{OH}$
	1471.8	1481.2		1476.8	
1755.3	1783.1	1792	1809.5	1789.8	$\nu_{C=O} + \delta_{OH}$
		1830.8		1802.3	
2671.8	2651.3	2666.3	2665.1	2609.7	ν_{SH}

	2670.8	2675.4		2651.2	
3093	3090	3051.8	3094.2	3095	ν_{sCH2}
	3099	3084.7			
3154.3	3150.8	3128.5	3157.6	3156.7	ν_{asCH2}
	3164.8	3153.3		3159.1	
3123	3355.2	3555	3568.5	3734.4	ν_{OH}
	3733.4	3736.7		3736.2	

[#]: ν = stretching, νs = symmetric stretching, νas = asymmetric stretching, δs = scissoring and δ = bending vibrational modes

Table 4.13c: Calculated IR vibrational modes (cm^{-1}) of TGA trimers (T1-T7) at B3LYP/cc-pVTZ//CCSD/cc-pVDZ level of theory

T1	T2	T3	T4	T5	T6	T7	Assignment[#]
671.2	668.3	671	695	694.6	685.8	680	$\nu_{CS} + \delta_{OCO}$
680.3	679.7	674.6	744.3	738.2	695.3	684.6	
697.2	698.5	682.5				694.4	
904	891	906.2	884.3	888.3	889.2	886.6	$\nu_{CC} + \delta_{COH}$
920.1	920	911.4	916.2	920.3	920	918.5	
932	928.3	917.3	921.2	924.8	925.3	922	
1289.3	1327	1299.8	1171	1145.6	1151.4	1147	$\nu_{CO} + \delta_{OH}$
1335.5	1357.2	1323	1341.5	1347.6	1346.4	1348.8	
1354	1414.1	1421.6	1400				
1471.1	1467.1	1454.1	1458.8	1448	1474.3	1469.3	δs_{CH2}
1484.6	1482.3	1470.3	1462.1	1484.1	1483	1487.7	
		1472.2					
1669.4	1675	1748	1756.1	1749.8	1750.6	1753.2	$\nu_{C=O} + \delta_{OH}$
1742	1742.3	1765.6	1791	1810.6	1790.3	1799.5	
1775.2	1803.4						
2643.1	2660.5	2667.4	2616.8	2611.2	2610.5	2664.1	ν_{SH}
2671	2668.8	2670.2	2652.2	2671.4	2644.5	2667	
	2672.1	2672	2667	2675.4	2671.3	2671.1	
3091.3	3091.7	3092.5	3061.3	3064.2	3093	3093	ν_{sCH2}
3094.2	3093.2	3093.6	3088.7	3093	3096.5	3095.1	
3098.5	3096.6		3092.2	3096.7			
3152	3153.6	3153	3113.1	3115.6	3154	3154.5	ν_{asCH2}
3155.6	3155.1	3155.1	3151.5	3154.2	3158.5	3161.3	
3161.6	3157.6		3156.2	3161	3160.6		
3012.7	2970.3	3192.6	2992.6	3011.1	3021.4	2995.8	ν_{OH}
3211.4	3251.3	3252.5	3511	3136.2	3735.3	3111.7	
3396	3415.5	3365.3		3744.3	3132.8	3737.6	

[#]: ν = stretching, νs = symmetric stretching, νas = asymmetric stretching, δs = scissoring and δ = bending vibrational modes

4.4 Conclusion

The conformational space of TGA was explored using the CCSD/cc-pVDZ level of theory. The most energetically favorable structure, referred to as GGC, was found as global minimum, in good agreement with the experimentally observed conformer. The second most stable conformer was also observed known as GAC conformer. The SH flipping barrier in TGA was found to be in good agreement with experimental observation suggesting low energy barrier. To examine sulfur-centered intermolecular hydrogen bonding, dimers and trimers of TGA were examined. Five stable dimers and seven stable trimers were optimized and evaluated using BSSE corrected interaction energy calculations. Among these structures, the D1 dimer and T1 trimer were found to be the most stable, displaying interaction energies of -14.64 kcal/mol and -22.87 kcal/mol, respectively, surpassing the other dimers and trimers in stability. And LED analysis using DLPNO-CCSD(T)/cc-pVTZ method revealed that the electrostatic correlation energy is the most significant contributor in interaction energy across all TGA clusters followed by exchange and dispersion correlation energy. These clusters exhibited intermolecular hydrogen bonding involving both oxygen and sulfur atoms, which contributed to their overall stability and cooperativity. The presence of these intermolecular hydrogen bond interactions in the dimers and trimers was confirmed through various analyses, including AIM (Atom in Molecules), RDG (Reduced Density Gradient), NBO (Natural Bond Orbital), and charge analysis. Furthermore, the existence of HBs was supported by the observation of a Red shift in the S-H stretching modes, as well as in O-H and C=O stretching modes, as determined by infrared (IR) frequency calculations.

4.5 References

(1) Vijayaraghavan, R.; Vedaraman, N.; Muralidharan, C.; Mandal, A. B.; Macfarlane, D. R. Aqueous Ionic Liquid Solutions as Alternatives for Sulphide-Free Leather Processing. *Green Chem.* **2015**, *17* (2), 1001–1007.

(2) Xie, N.; Ding, X.; Wang, X.; Wang, P.; Zhao, S.; Wang, Z. Determination of Thioglycolic Acid in Cosmetics by Capillary Electrophoresis. *J. Pharm. Biomed. Anal.* **2014**, *88*, 509–512.

(3) Liu, Y.; Li, H.; Shu, W.; Chen, Q. Synthesis and Application of Antimony Pent (Isooctyl Thioglycollate). *J. Cent. South Univ. Technol.* **2005**, *12*, 64–67.

(4) Mousaa, I.; Radi, H. Comparative Studies of Anticorrosion Performance of Novel Inhibitors Based on Oleic Acid and Sulfur/Nitrogen Containing Compounds in UV-Curable Coatings. *Corros. Eng. Sci. Technol.* **2017**, *52* (7), 547–556.

(5) Xia, L.; Hou, S.; Ren, X.; Wang, Z. Effects of Thioglycolic Acid on in Vivo Oocytes Maturation in Mice. *Plos One* **2011**, *6* (9), e23996.

(6) Gan, H.-F.; Meng, X.-S.; Song, C.-H.; Li, B.-X. A Survey on Health Effects in a Human Population Exposed to Permanent-Waving Solution Containing Thioglycolic Acid. *J. Occup. Health* **2003**, *45* (6), 400–404.

(7) Summonte, S.; Racaniello, G. F.; Lopedota, A.; Denora, N.; Bernkop-Schnürch, A. Thiolated Polymeric Hydrogels for Biomedical Application: Cross-Linking Mechanisms. *J. Controlled Release* **2021**, *330*, 470–482.

(8) Koç, Ö. K.; Üzer, A.; Apak, R. A Colorimetric Probe Based on 4-Mercaptophenol and Thioglycolic Acid-Functionalized Gold Nanoparticles for Determination of Phytic Acid and Fe (III) Ions. *Microchim. Acta* **2020**, *187*, 1–13.

(9) Kumar, A.; Dutta, R. K. CdS Quantum Dots Immobilized on Calcium Alginate Microbeads for Rapid and Selective Detection of Hg 2+ Ions. *RSC Adv.* **2015**, *5* (93), 76275–76284.

(10) Shetty, P.; Nityananda, S.; Gadag, R.; others. Indirect Complexometric Determination of Thallium (III) Using Thioglycolic Acid as Masking Agent. **2000**.

(11) Devi, R.; Khatkar, S. Thioglycolic Acid as an Amperometric Reagent for Trace Determination of Co (II) and Ni (II). *Asian J. Chem.* **2007**, *19* (6), 4373.

(12) Kenawy, I.; Abou El-Reash, Y.; Hassanien, M.; Alnagar, N.; Mortada, W. Use of Microwave Irradiation for Modification of Mesoporous Silica Nanoparticles by Thioglycolic Acid for Removal of Cadmium and Mercury. *Microporous Mesoporous Mater.* **2018**, *258*, 217–227.

(13) Lowe, A. B. Thiol–Ene "Click" Reactions and Recent Applications in Polymer and Materials Synthesis: A First Update. *Polym. Chem.* **2014**, *5* (17), 4820–4870.

(14) Kondratenko, T.; Ovchinnikov, O.; Grevtseva, I.; Smirnov, M.; Erina, O.; Khokhlov, V.; Darinsky, B.; Tatianina, E. Thioglycolic Acid FTIR Spectra on Ag2S Quantum Dots Interfaces. *Materials* **2020**, *13* (4), 909.

(15) Hussain, A.; Pu, H.; Hu, B.; Sun, D.-W. Au@ Ag-TGANPs Based SERS for Facile Screening of Thiabendazole and Ferbam in Liquid Milk. *Spectrochim. Acta. A. Mol. Biomol. Spectrosc.* **2021**, *245*, 118908.

(16) Nguyen, K. C. Quantitative Analysis of COOH-Terminated Alkanethiol SAMs on Gold Nanoparticle Surfaces. *Adv. Nat. Sci. Nanosci. Nanotechnol.* **2012**, *3* (4), 045008.

(17) Yamaguchi, I.; Hasegawa, H.; Hirono, H.; Aizawa, Y.; Takagi, M.; Watanabe, H.; Sekiguchi, T.; Kobayashi, H.; Terasawa, H.; Watanabe, K. An Interpretation of the Microwave Spectrum of Mercaptoacetic Acid. *J. Mol. Spectrosc.* **1995**, *172* (1), 296–298.

(18) Caminati, W.; Maris, A.; Favero, P. G. Free Jet Absorption Millimeter-Wave Spectrum of Thioglycolic Acid. *J. Mol. Spectrosc.* **1996**, *175* (1), 215–216.

(19) Fantoni, A. CONFORMATIONAL AND DYNAMICAL PROPERTIES OF THE C (O)–CH2–S–H MOIETY IN THIOGLYCOLIC ACID AND METHYLTHIOGLYCOLATE: AN AB INITIO AND DFT STUDY. *J. Theor. Comput. Chem.* **2002**, *1* (02), 309–317.

(20) Gerlt, J. A.; Kreevoy, M. M.; Cleland, W.; Frey, P. A. Understanding Enzymic Catalysis: The Importance of Short, Strong Hydrogen Bonds. *Chem. Biol.* **1997**, *4* (4), 259–267.

(21) Perrin, C. L.; Nielson, J. B. "Strong" Hydrogen Bonds in Chemistry and Biology. *Annu. Rev. Phys. Chem.* **1997**, *48* (1), 511–544.

(22) Fersht, A. R. The Hydrogen Bond in Molecular Recognition. *Trends Biochem. Sci.* **1987**, *12*, 301–304.

(23) Harding, S. E.; Channell, G.; Phillips-Jones, M. K. The Discovery of Hydrogen Bonds in DNA and a Re-Evaluation of the 1948 Creeth Two-Chain Model for Its Structure. *Biochem. Soc. Trans.* **2018**, *46* (5), 1171–1182.

(24) Perlstein, J. The Weak Hydrogen Bond In Structural Chemistry and Biology (International Union of Crystallography, Monographs on Crystallography, 9) By Gautam R. Desiraju (University of Hyderabad) and Thomas Steiner (Freie Universität Berlin). Oxford University Press: Oxford and New York. 1999. Xiv+ 507 Pp. $150. ISBN 0-19-850252-4., 2001.

(25) Desiraju, G. R.; Steiner, T. *The Weak Hydrogen Bond: In Structural Chemistry and Biology*; International Union of Crystal, 2001; Vol. 9.

(26) Zhou, P.; Tian, F.; Lv, F.; Shang, Z. Geometric Characteristics of Hydrogen Bonds Involving Sulfur Atoms in Proteins. *Proteins Struct. Funct. Bioinforma.* **2009**, *76* (1), 151–163.

(27) Biswal, H. S.; Bhattacharyya, S.; Bhattacherjee, A.; Wategaonkar, S. Nature and Strength of Sulfur-Centred Hydrogen Bonds: Laser Spectroscopic Investigations in the Gas Phase and Quantum-Chemical Calculations. *Int. Rev. Phys. Chem.* **2015**, *34* (1), 99–160.

(28) Chand, A.; Sahoo, D. K.; Rana, A.; Jena, S.; Biswal, H. S. The Prodigious Hydrogen Bonds with Sulfur and Selenium in Molecular Assemblies, Structural Biology, and Functional Materials. *Acc. Chem. Res.* **2020**, *53* (8), 1580–1592.

(29) Arunan, E.; Emilsson, T.; Gutowsky, H.; Fraser, G. T.; De Oliveira, G.; Dykstra, C. Rotational Spectrum of the Weakly Bonded C 6 H 6–H 2 S Dimer and Comparisons to C 6 H 6–H 2 O Dimer. *J. Chem. Phys.* **2002**, *117* (21), 9766–9776.

(30) Goswami, M.; Arunan, E. Microwave Spectrum and Structure of C6H5CCH⋯ H2S Complex. *J. Mol. Spectrosc.* **2011**, *268* (1–2), 147–156.

(31) Lobo, I. A.; Robertson, P. A.; Villani, L.; Wilson, D. J.; Robertson, E. G. Thiols as Hydrogen Bond Acceptors and Donors: Spectroscopy of 2-Phenylethanethiol Complexes. *J. Phys. Chem. A* **2018**, *122* (36), 7171–7180.

(32) Liakos, D. G.; Neese, F. Is It Possible to Obtain Coupled Cluster Quality Energies at near Density Functional Theory Cost? Domain-Based Local Pair Natural Orbital

Coupled Cluster vs Modern Density Functional Theory. *J. Chem. Theory Comput.* **2015**, *11* (9), 4054–4063.

(33) Altun, A.; Neese, F.; Bistoni, G. Local Energy Decomposition Analysis of Hydrogen-Bonded Dimers within a Domain-Based Pair Natural Orbital Coupled Cluster Study. *Beilstein J. Org. Chem.* **2018**, *14* (1), 919–929.

(34) Reva, I. D.; Jarmelo, S.; Lapinski, L.; Fausto, R. First Experimental Evidence of the Third Conformer of Glycolic Acid: Combined Matrix Isolation, FTIR and Theoretical Study. *Chem. Phys. Lett.* **2004**, *389* (1–3), 68–74.

(35) Yamaguchi, I.; Hasegawa, H.; Hirono, H.; Aizawa, Y.; Takagi, M.; Watanabe, H.; Sekiguchi, T.; Kobayashi, H.; Terasawa, H.; Watanabe, K. An Interpretation of the Microwave Spectrum of Mercaptoacetic Acid. *J. Mol. Spectrosc.* **1995**, *172* (1), 296–298.

(36) Bolton, K.; Sheridan, J. Microwave Spectrum of Propargyl Mercaptan; Observation of Predominantly Vibrational Transitions of the Torsion Mode. *Spectrochim. Acta Part Mol. Spectrosc.* **1970**, *26* (5), 1001–1006.

(37) Kojima, T. Microwave Spectrum of Methyl Mercaptan. **1960**, *15* (7), 1284–1291. https://doi.org/10.1143/JPSJ.15.1284.

(38) Lees, R.; Baker, J. Torsion–Vibration–Rotation Interactions in Methanol. I. Millimeter Wave Spectrum. *J. Chem. Phys.* **1968**, *48* (12), 5299–5318.

(39) Fantoni, A. CONFORMATIONAL AND DYNAMICAL PROPERTIES OF THE C (O)–CH2–S–H MOIETY IN THIOGLYCOLIC ACID AND METHYLTHIOGLYCOLATE: AN AB INITIO AND DFT STUDY. *J. Theor. Comput. Chem.* **2002**, *1* (02), 309–317.

(40) Rezac, J.; Hobza, P. Describing Noncovalent Interactions beyond the Common Approximations: How Accurate Is the "Gold Standard," CCSD (T) at the Complete Basis Set Limit? *J. Chem. Theory Comput.* **2013**, *9* (5), 2151–2155.

(41) Rezac, J.; Simova, L.; Hobza, P. CCSD [T] Describes Noncovalent Interactions Better than the CCSD (T), CCSD (TQ), and CCSDT Methods. *J. Chem. Theory Comput.* **2013**, *9* (1), 364–369.

(42) Ramabhadran, R. O.; Raghavachari, K. Extrapolation to the Gold-Standard in Quantum Chemistry: Computationally Efficient and Accurate CCSD (T) Energies for Large Molecules Using an Automated Thermochemical Hierarchy. *J. Chem. Theory Comput.* **2013**, *9* (9), 3986–3994.

(43) Hobza, P.; Zahradník, R.; STULIKOVA, M. Intermolecular Complexes: The Role of van Der Waals Systems in Physical Chemistry and in the Biodisciplines. *Stud. Phys. Theor. Chem.* **1988**, *52*, 1–307.

(44) Van Duijneveldt, F. B.; van Duijneveldt-van de Rijdt, J. G.; van Lenthe, J. H. State of the Art in Counterpoise Theory. *Chem. Rev.* **1994**, *94* (7), 1873–1885.

(45) Van Lenthe, J. J-G-C-M. van Duijneveldt-van de Rijdt and FB v,∼ n Dt1ijneveldt, Adv. *Chern Pbys* **1987**, *79*, 521.

(46) Boys, S. F.; Bernardi, F. The Calculation of Small Molecular Interactions by the Differences of Separate Total Energies. Some Procedures with Reduced Errors. *Mol. Phys.* **1970**, *19* (4), 553–566.

(47) Sum, A. K.; Sandler, S. I. Ab Initio Calculations of Cooperativity Effects on Clusters of Methanol, Ethanol, 1-Propanol, and Methanethiol. *J. Phys. Chem. A* **2000**, *104* (6), 1121–1129.

(48) Schneider, W. B.; Bistoni, G.; Sparta, M.; Saitow, M.; Riplinger, C.; Auer, A. A.; Neese, F. Decomposition of Intermolecular Interaction Energies within the Local Pair Natural Orbital Coupled Cluster Framework. *J. Chem. Theory Comput.* **2016**, *12* (10), 4778–4792.

(49) Altun, A.; Saitow, M.; Neese, F.; Bistoni, G. Local Energy Decomposition of Open-Shell Molecular Systems in the Domain-Based Local Pair Natural Orbital Coupled Cluster Framework. *J. Chem. Theory Comput.* **2019**, *15* (3), 1616–1632.

(50) Altun, A.; Neese, F.; Bistoni, G. Effect of Electron Correlation on Intermolecular Interactions: A Pair Natural Orbitals Coupled Cluster Based Local Energy Decomposition Study. *J. Chem. Theory Comput.* **2018**, *15* (1), 215–228.

(51) Jaworski, A.; Hedin, N. Local Energy Decomposition Analysis and Molecular Properties of Encapsulated Methane in Fullerene (CH 4@ C 60). *Phys. Chem. Chem. Phys.* **2021**, *23* (38), 21554–21567.

(52) Neese, F.; Wennmohs, F.; Becker, U.; Riplinger, C. The ORCA Quantum Chemistry Program Package. *J. Chem. Phys.* **2020**, *152* (22).

(53) Lu, T.; Chen, F. Multiwfn: A Multifunctional Wavefunction Analyzer. *J. Comput. Chem.* **2012**, *33* (5), 580–592.

(54) Humphrey, W.; Dalke, A.; Schulten, K. VMD: Visual Molecular Dynamics. *J. Mol. Graph.* **1996**, *14* (1), 33–38.

(55) Emamian, S.; Lu, T.; Kruse, H.; Emamian, H. Exploring Nature and Predicting Strength of Hydrogen Bonds: A Correlation Analysis between Atoms-in-Molecules Descriptors, Binding Energies, and Energy Components of Symmetry-Adapted Perturbation Theory. *J. Comput. Chem.* **2019**, *40* (32), 2868–2881.

(56) Espinosa, E.; Molins, E.; Lecomte, C. Hydrogen Bond Strengths Revealed by Topological Analyses of Experimentally Observed Electron Densities. *Chem. Phys. Lett.* **1998**, *285* (3–4), 170–173.

(57) Singh, U. C.; Kollman, P. A. An Approach to Computing Electrostatic Charges for Molecules. *J. Comput. Chem.* **1984**, *5* (2), 129–145.

(58) Subashchandrabose, S.; Saleem, H.; Erdogdu, Y.; Rajarajan, G.; Thanikachalam, V. FT-Raman, FT-IR Spectra and Total Energy Distribution of 3-Pentyl-2, 6-Diphenylpiperidin-4-One: DFT Method. *Spectrochim. Acta. A. Mol. Biomol. Spectrosc.* **2011**, *82* (1), 260–269.

(59) Helgaker, T.; Jorgensen, P.; Olsen, J. *Molecular Electronic-Structure Theory*; John Wiley & Sons, 2013.

(60) Esrafili, M. D.; Behzadi, H.; Hadipour, N. L. Theoretical Study of N–H⋯ O Hydrogen Bonding Properties and Cooperativity Effects in Linear Acetamide Clusters. *Theor. Chem. Acc.* **2008**, *121* (3–4), 135–146.